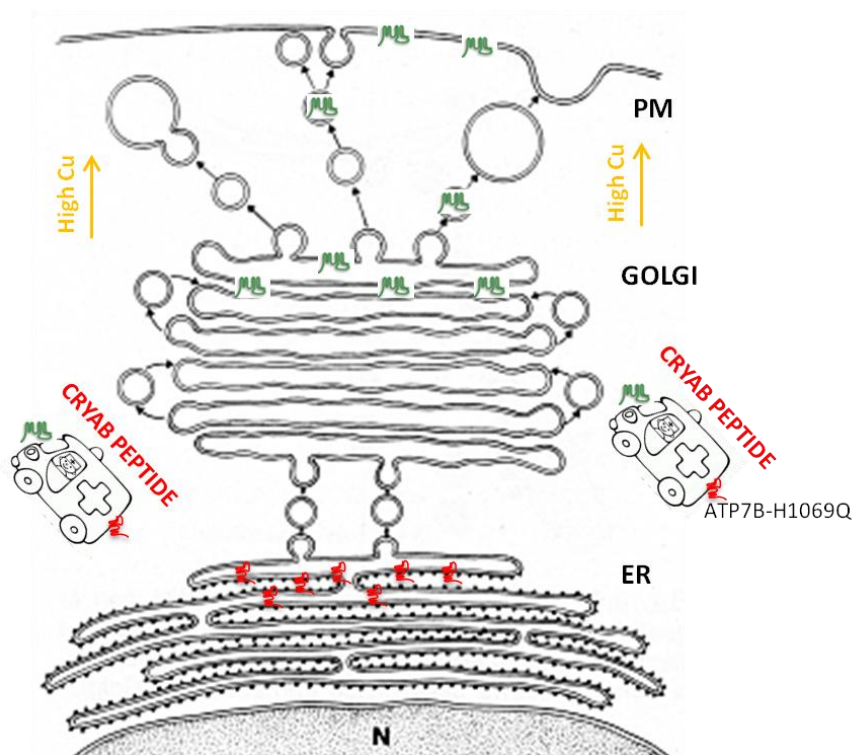


UNIVERSITY OF NAPLES FEDERICO II

DOCTORATE
MOLECULAR MEDICINE AND MEDICAL BIOTECHNOLOGY

XXX CYCLE

**New Therapeutic Perspectives for the Most Frequent
ATP7B Mutation in Wilson Disease: Development of
Pharmacologically Active Peptides and Generation of
a Novel WD Isogenic Cell Model**



Academic Year 2016/2017

UNIVERSITY OF NAPLES FEDERICO II

**DOCTORATE
MOLECULAR MEDICINE AND MEDICAL BIOTECHNOLOGY**

XXX CYCLE



**New Therapeutic Perspectives for the Most Frequent
ATP7B Mutation in Wilson Disease: Development of
Pharmacologically Active Peptides and Generation of
a Novel WD Isogenic Cell Model**

Mentor
Prof. Stefano Bonatti

Candidate
Dr. Simona Allocca

COORDINATOR
Prof. Vittorio Enrico Avvedimento

Academic Year 2016/2017

INDEX

ABSTRACT	1
Abbreviations	
1. INTRODUCTION	4
1.1 - Copper fate in human metabolism	
1.2 - Wilson disease: hallmarks of molecular pathogenesis	
1.3 - ATP7B: molecular architecture and function	
1.4 - H1069Q: the most frequent ATP7B mutation among Caucasians	
1.5 - Multifunctional cellular properties of αB-crystallin protein	
1.6 - Phosphorylation modulates both the structural and functional properties of CRYAB	
1.7 - CRYAB-derived peptide: therapeutic perspectives for conformational diseases	
1.8 - Wilson disease models	
2. AIM OF THE THESIS	19
3. MATERIALS AND METHODS	20
4. RESULTS	29
4.1 - α-crystallin domain is able to rescue the physiological localization of ATP7B-H1069Q	
4.2 - CRYAB-derived peptide does not affect cell viability	

- 4.3 - CRYAB peptide is mainly cytosolic and associated with vesicular compartments in a time-dependent manner
- 4.4 - Comparing the effect of CRYAB peptide on the localization of ATP7B-H1069Q in COS-7, Hep-G2 KO, and Huh-7 cell lines
- 4.5 - Golgi-corrected ATP7B-H1069Q redistributes to post Golgi vesicles in response to copper overload
- 4.6 - CRYAB peptide interacts with ATP7B-H1069Q
- 4.7 - Differentiation toward hepatocytes of iPSCs obtained by reprogramming skin fibroblasts from a WD patient and his mother (control)
- 4.8 - ATP7B shows both a reticular and Golgi localization and is degraded faster in patient HLCs than in control HLCs
- 4.9 - Golgi ATP7B pool responds to increasing copper levels in patient HLCs

5. CONCLUSIONS AND DISCUSSION	51
6. ACKNOWLEDGEMENTS	57
7. REFERENCES	58
8. LIST OF PUBLICATIONS	71

ABSTRACT

Background

Wilson Disease (WD) is an autosomal recessive inherited disorder, which if left untreated can be lethal. Its development is due to abnormal copper (Cu) metabolism. In particular, reduced copper excretion causes an excessive deposition of the ion in many organs such as the liver, central nervous system, cornea, kidney, and cardiac muscle, thereby damaging the physiological functions of the affected organs. Mutations in the P-type adenosine triphosphatase (*ATP7B*), the gene encoding the copper transporting P-type ATPase, are responsible for hepatic copper accumulation. Cu overload in the liver produces toxic effects via modulating several molecular pathways.

The recessive *ATP7B*-H1069Q mutation alone is the most frequent cause of WD among Caucasians (~60%). Physiologically, *ATP7B* transfers copper across the membrane into the lumen of the *trans*-Golgi network (TGN). In the Golgi, the metal is incorporated into the serum protein ceruloplasmin (CP). In the presence of excessive cytosolic Cu, the metal is localized by *ATP7B* to post-Golgi vesicles and plasma membrane (PM), where it is removed via bile canaliculi.

Overexpression studies in heterologous cell systems show that H1069Q mutation results in aberrant protein products that are strongly mis-targeted from the TGN towards the endoplasmic reticulum (ER). Despite that, this mutant still exhibits residual Cu translocating activity, which might be sufficient enough to ward off the disease if the protein is correctly localized to the TGN. In this context, our previous work has demonstrated that the cytosolic holdase α B-crystallin (CRYAB or Hsp-B5) rescues the proper folding, localization and response to Cu overload of *ATP7B*-H1069Q in Hep-G2 and COS-7 cells.

Rationale

Evidence that residual Cu transport activity is retained by *ATP7B*-H1069Q and that correcting agents can indeed localize this mutant to the Golgi complex has spurred our great interest in investigating the potentially therapeutic implications of these findings.

My PhD thesis describes the properties of a CRYAB-derived mini-chaperone in heterologous or hepatoma-derived cell lines overexpressing *ATP7B*-H1069Q and the generation of an isogenic cell model based on induced pluripotent stem cells (iPSCs) created from skin fibroblasts of a homozygous WD patient and his mother, used as control, followed by differentiation into hepatocyte-like cells (HLCs).

Main results

We found that the CRYAB peptide enters the cytosol and only a small fraction is associated with lysosome structures. The peptide interacts with ATP7B-H1069Q, rescuing its Golgi localization and trafficking response to increased Cu level.

Other important results, obtained by virtue of our new WD cell model are the following: 1) the expression level of the mutant protein in HLCs was only 30% compared to the control, although ATP7B mRNA levels were similar; 2) a significant amount of ATP7B-H1069Q (about 35%) reached the Golgi complex and was able to redistribute to the endo/lysosomal compartment in the presence of Cu excess; 3) most of the newly synthesized mutant underwent rapid ER-associated degradation.

Conclusion

Biochemical optimization of the CRYAB peptide could provide helpful insights into its mechanism of action and its potential use for WD treatment. Meanwhile, the new isogenic WD cell model is a powerful system to validate *in vitro* results, obtained in heterologous or hepatoma-derived cell lines. In this context, ATP7B-H1069Q dysfunction could be tackled by treatments that reduce ER-associated degradation, thereby increasing the number of molecules reaching the TGN.

Abbreviations:

albumin, ALB
ceruloplasmin, CP
co-immunoprecipitation, co-IP
copper, Cu
C-terminal extension, CTE
endoplasmic reticulum, ER
fluorescence energy transfer, FRET
fluorescence lifetime imaging microscopy, FLIM
hepatocyte-like cells, HLCs
induced pluripotent stem cells, iPSCs
late endosome, LE
Menkes disease, MD
N-terminal domain, NTD
nucleotide binding domain, NBD
plasma membrane, PM
quantitative real-time RT-PCR, qPCR
selected ion monitoring mass spectrometry, SIM-MS
tetramethylrhodamine, TAMRA
trans-Golgi network, TGN
Wilson disease, WD
 α 1-antitrypsin, AAT
 α B-crystallin, CRYAB
 α -crystallin domain, CD

1. INTRODUCTION

1.1 *Copper fate in human metabolism*

The human body comprises a sophisticated and delicate homeostatic balance of trace elements indispensable for the preservation of all cellular processes. Therefore, excessive accumulation or deficiency of these elements must be prevented.

Copper is an emblematic example of such trace elements. It is a cofactor of key metabolic enzymes that are involved in antioxidant defence, mitochondrial respiration, neurotransmitter synthesis, connective tissue formation, pigmentation, peptide amidation, iron metabolism and many other physiological pathways (Table1) (1, 2).

The average daily intake of copper is between 1 and 3 mg, an amount adequate for body needs. Although it is well known that the majority of Cu adsorption takes place in the duodenum, the molecular mechanisms of dietary copper assimilation remain quite elusive. So far, studies have shown that Cu enters enterocytes mainly through the high-affinity copper transporter *Ctr1* even though other pathways/transporters might also be involved. Once inside the enterocytes, it is exported into the blood by Cu-ATPase *ATP7A* (Fig. 1) (2). Here, the majority of copper is delivered to the liver (3), and to a lesser extent to the kidney and other tissues (4). The liver is indeed the central organ of copper homeostasis and is primarily responsible for the export of excess copper out of the body (2).

In contrast to the low regulation of Cu uptake into the liver, the export mechanism from this organ is a highly regulated copper-dependent process, which is mediated by copper-transporting ATPase *ATP7B*. It is from the hepatocytes that copper is distributed to various intracellular destinations (Fig. 2).

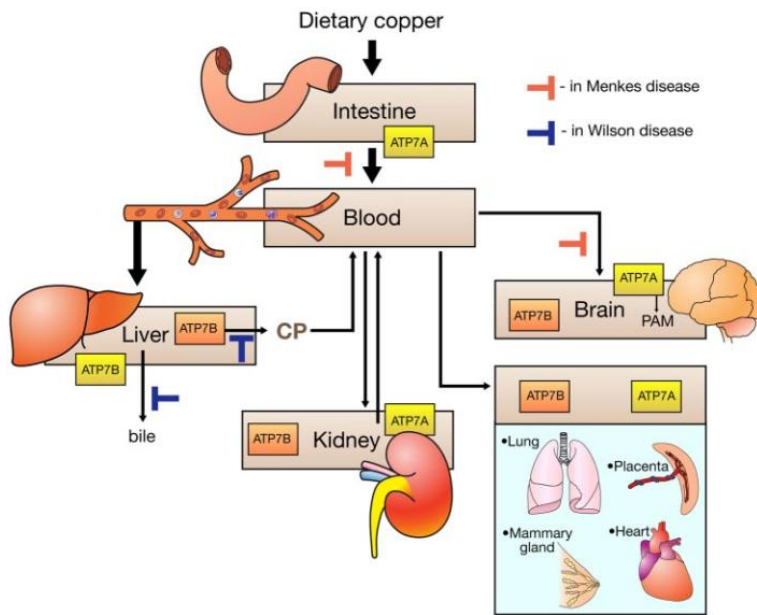
The first destination is the cytosol. Here, it is utilized by a radical-detoxifying enzyme copper, zinc-dependent superoxide dismutase (*SOD1*), which acquires copper with the help of a specific metallochaperone, *viz.*, the copper chaperone of superoxide dismutase (*CCS*) (5). Then it enters the mitochondria. Here, it is incorporated into cytochrome-*c* oxidase (*COX*) (6, 7, 8). Lastly, it reaches its major destination: the trans-Golgi network (*TGN*). This secretory pathway contains Cu-ATPases (*ATP7B* in hepatocyte), which receive the metal from the cytosolic copper transporter *Atox1* (9, 10, 11) and transfer it across the membrane into the lumen of the *TGN*. In hepatocytes, it is incorporated into the copper-dependent ferroxidase ceruloplasmin (*CP*). *CP* is subsequently secreted into the blood, therefore making this protein the major copper containing protein in blood serum (Fig. 1). In addition to *CP*, *ATP7B* is also required for the elimination of excess copper. This protein

facilitates excess Cu into bile through the relocalization towards the LE/lysosomal compartment and the plasma membrane of bile canaliculi (2). Therefore, the copper-transporting P-type ATPases exert a key role in regulating copper metabolism. Mutations in ATP7A or ATP7B disrupt the homeostatic copper balance, causing severe metabolic disorders.

Enzyme	Function	Consequences of deficiency
Caeruloplasmin	Iron and copper transport	Decreased circulating copper levels, iron deficiency
Cytochrome C oxidase	Mitochondrial respiration	Hypothermia, muscle weakness
Dopamine β -hydroxylase	Catecholamine production	Hypothermia, neurological defects
Lysyl oxidase	Connective tissue formation	Laxity of skin and joints
Peptidylglycine α -amidating mono-oxygenase	Peptide amidation	Neuroendocrine defects
Superoxide dismutase	Antioxidant defence	Diminished protection against oxidative stress
Tyrosinase	Pigment formation	Hypopigmentation of hair and skin

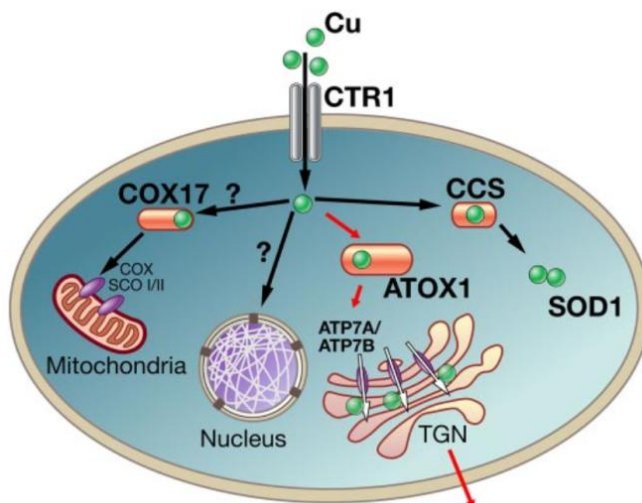
(P de Bie et al., 2007)

Table 1. Functions of copper-dependent enzymes.



(S. Lutsenko et al., 2007)

Fig. 1. Scheme of copper distribution in the human body.



(S. Lutsenko et al., 2007)

Fig. 2. Intracellular pathways of copper distribution. Ctr1 transports Cu into the cell. Cox17 may participate in delivery of copper to mitochondrion and, together with Sco proteins, facilitates Cu incorporation into COX. CCS transfers copper to cytosolic SOD1. The red arrows indicate the pathway in which Cu-ATPases are involved. They receive copper from ATOX1, transfer it into the lumen of TGN, and export excess copper from the cell.

1.2 Wilson disease: hallmarks of molecular pathogenesis

Refined mechanisms have evolved to control intake, excretion, and cellular distribution of copper. The importance of these regulatory processes is underlined by several hereditary human disorders caused by imbalances of copper homeostasis. These disorders can broadly be divided into two classes: diseases associated with copper deficiency and diseases associated with copper excess (1).

A copper-deficiency disease is Menkes disease (MD). MD is an X-linked recessive disorder characterized by a general copper deficiency (12, 13) due to mutations or deletions in the gene encoding Cu-ATPase ATP7A (2).

Its incidence is estimated to range between 1:40000 and 1:350000 (14, 15, 16). Affected patients display dramatic developmental and neurological impairment due to the disrupted delivery of Cu to the brain (17). Moreover, they suffer from a variety of other symptoms that are associated with decreased function of Cu-dependent enzymes, including connective tissue

alterations, lack of pigmentation, and tortuous blood vessels (17, 18, 19). The majority of MD patients die in early childhood.

On the other hand, Wilson disease (WD), also known as hepatolenticular degeneration, is an autosomal recessive disorder characterized by defective copper excretion that leads to the deposition of copper and the impairment of the normal functions of the affected organs (20). First described by Wilson in 1912 but not yet clearly characterized, WD has an incidence of 1:7000 live births (21).

Clinical features of WD result from toxic accumulation of copper, primarily in the liver and the brain (1). The accumulation in the brain may cause Parkinson-like symptoms, including tremor, and dystonia, or neuropsychiatric symptoms, such as hypomnesia, and personality abnormalities (22, 23). The Kayser-Fleischer (KF) ring, a brown ring around the cornea of the eye, is the result of ion accumulation in the cornea. Although it is a hallmark of WD, it is not diagnostic for the disease. Copper deposition in other organs may cause corresponding clinical disorders: osteoarthritis, impaired kidney function, and cardiomyopathy (24).

Liver is the major organ for copper deposition in patients with WD. Excess copper causes a large spectrum of hepatic dysfunctions ranging from mild abnormalities in liver function to acute or chronic hepatitis and cirrhosis (25). In some severe cases, patients present with fulminant liver failure (1).

In addition, WD patients often have reduced serum levels of the cuproenzyme caeruloplasmin as a result of rapid degradation of the copper free form of CP (26, 27).

ATP7B is the key culprit gene for WD. Mutations in the *ATP7B* gene are closely linked to abnormal copper excretion, leading to excessive deposition of copper in the target organs (28). Almost 300 *ATP7B* mutations have been associated with WD development (29), of which up to 60% are missense mutations (30). Although most WD-causing mutations are rare, some are more common than others and account for a large portion of WD cases. In particular, the most prevalent ones are H1069Q in Europe and North America, and R778L in southeast Asia (31).

Wilson disease is characterized by extensive clinical heterogeneity, even among patients with the same mutations. The main differences lie in the age at presentation, severity of the disease, and the predominance of hepatic versus neurological symptoms (27).

There are two therapeutic approaches to counter WD: copper chelation treatment using penicillamine or trientine (32), and zinc therapy. Zinc induces enterocyte metallothionein, a cysteine-rich protein that is an endogenous metal chelator (24). Controversy exists as to which approach constitutes the more effective treatment regimen; however, when pharmacological treatments fail, or fulminant liver failure develops, liver

transplantation remains the only viable option (1). The major disadvantage of these therapies is the development of serious adverse effects. For instance, Cu-chelating agents induce serious toxicities, including hypersensitivity reactions, development of autoimmune disease, and bone marrow suppression. Zinc therapies are not exempt from adverse effects either. Therefore, there is a clear demand for novel WD treatment strategies.

1.3 *ATP7B: molecular architecture and function*

ATP7B belongs to the P-type ATPase family gene and is located on chromosome 13q.14.3 (33). The gene consists of 20 introns and 21 exons and several domains contribute to its critical function.

ATP7B is a multispan transmembrane (TM) protein of 1465 aa that contains 8 TM segments that form a channel for Cu translocation and 7 short luminal loops that connects these TM segments. The Cys-Pro-Cys (CPC) sequence motif, in the sixth transmembrane domain, is highly conserved across all ATPases. Moreover, since it is thought to be part of the intramembrane metal-binding site, studies suggest that it promotes copper transportation (34, 35). In the N-terminal domain, there are 6 metal-binding domains (MBDs), each of which contains the repetitive sequence motif GMXCXXC. The MBDs have high affinity for copper and play a major role in the acceptance of metal from the cytosolic copper transporter Atox1 by special protein-protein interactions (36). Mutation analysis has proven that MBD5 and MBD6 can influence the catalysis and activation of *ATP7B* activity, whereas MBD1-4 have less impact on *ATP7B* (37).

ATP7B contains an ATP-binding domain (N-domain or NBD), a phosphorylation domain (P-domain), and a phosphatase domain (A-domain) (38).

NBD participates in domain-domain interactions (39) and contains a unique and highly conserved amino acid motif, SEHPL, (histidine is an invariant residue) (40). Interestingly, although it is still unclear how SEHPL motif influences copper transport, its mutation (His1069Q) represents the most common WD mutation among Northern European populations (40).

In the P-domain, a highly conserved motif, DKTGT, is crucial for the enzymatic phosphorylation occurring at the aspartic acid residue of the sequence (41). In particular, acyl-phosphate is the phosphorylated intermediate that drives protein conformational changes and copper transport to the opposite site of the membrane (42). In the A-domain, acyl-phosphate is dephosphorylated. The phosphatase activity is due to the Glu residue in the

Thr-Gly-Glu sequence motif (TGE) of the A-domain. Dephosphorylation, instead, marks the completion of the cycle (20).

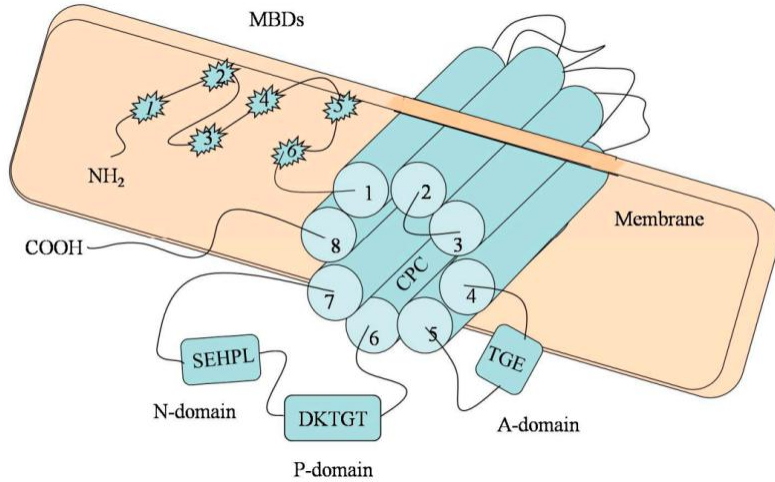
Although the C-terminal domain is dispensable for catalysis, it is indispensable for maintaining protein stability and for regulating protein localization (34, 43). Wilson disease-associated mutations have been identified in the COOH terminus of ATP7B, indicating that this region has significant structural and/or regulatory properties. Indeed, some of these mutants are unstable, fail to be retained in the Golgi in low copper, and are unresponsive to the addition of copper (44).

The structure of ATP7B is schematically illustrated in Fig. 3.

ATP7B is expressed in most organs and, to a much greater extent, in the liver. Intracellularly, ATP7B is mainly localized in the TGN (45, 46). More recent studies have indicated that ATP7B is redistributed from TGN to the late endosome/lysosome and plasma membrane of bile canaliculi when copper concentrations rise (47, 48).

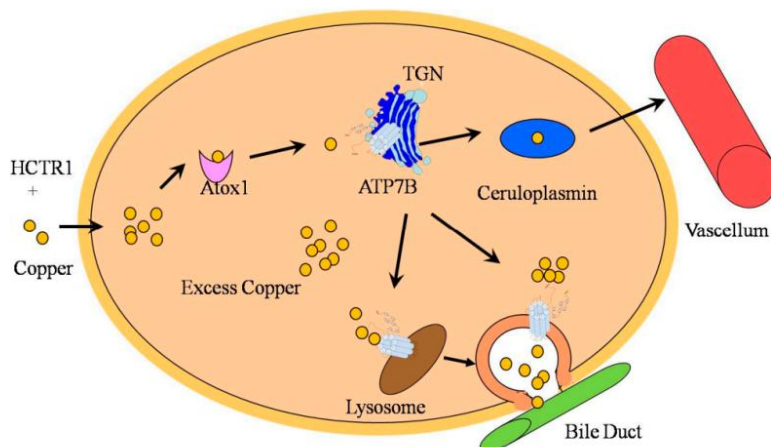
Therefore, ATP7B plays a double role in the liver. On one hand, it participates in copper transportation to TGN where copper is incorporated into ceruloplasmin, and, on the other hand, it drives excess copper from the liver into the bile ducts for excretion (20) (Fig. 4).

Excess copper facilitates ATP7B trafficking from the TGN to the lysosome, thereby facilitating the subsequent import of copper into the lysosomal lumen. Once the level of copper reaches a threshold value, toxic copper is excreted into bile via exocytosis (49). Moreover, increased copper levels can also stimulate ATP7B to move into the cytosolic vesicles, where copper may be “isolated” to protect cells from metal induced toxicity. Copper in vesicles is thought to be excreted by a similar mechanism as in the lysosomes (exocytosis) (50).



(Fei Wu et al., 2015)

Fig. 3. Diagram of ATP7B. The metal-binding domain consists of 6 copper-binding domains (MBD1-6), all with the conserved sequence motif CXXC. The transmembrane channel is composed of 8 discontinuous ion channels (Cylinder 1-8). The Cys-Pro-Cys (CPC) sequence motif confers metal ion selectivity. ATP binds to the N-domain and the SEHPL motif located in the N-domain. The P-domain is required for phosphorylation of Asp in the sequence DKTGT. The A-domain is the place where the acyl-phosphate is dephosphorylated.



(Fei Wu et al., 2015)

Fig. 4. Schematic illustration of copper transport and metabolism. HCTR1 delivers copper to the cytosol. Atox1 transfers the metal to TGN and is transported into the lumen with the help of ATP7B. Copper is then incorporated into ceruloplasmin secreted into the blood. The excess copper induces ATP7B trafficking from the TGN to the lysosome, from where it is transported to the lysosomal lumen. The excess copper is thus excreted into bile via exocytosis. A copper overload also stimulates ATP7B to move to cytosolic vesicles where copper is isolated and then released into the bile duct.

1.4 H1069Q: the most frequent ATP7B mutation among Caucasians

Nearly 500 mutations in ATP7B have been identified. Among these, more than 300 mutations have been found to be associated with WD (51). Mutations may occur at any position of the gene and the most common form of ATP7B mutation is missense mutation. Generally, frameshift and missense mutations are associated with a more severe phenotype of WD (52).

It has been demonstrated that a genetic heterogeneity in patients with WD exists across various races and geographical regions (53). For example, H1069Q mutation of the ATP7B is more prevalent (about 60%) in WD patients of European origin, including Italians, Romanians, and Swedish, (54), whereas the R778L mutation is more common in East Asia (55). Therefore, both the variability in ATP7B mutation and gene heterozygosity make it difficult to use mutation signatures as a diagnostic tool (56).

WD-associated mutations affect the intracellular trafficking of ATP7B and/or its ability to transfer Cu across the membrane (1, 2, 57).

In particular, H1069Q is defined as a mild mutation because it results in aberrant protein products that are strongly mis-targeted from the TGN towards the ER (Fig. 5) (58); however, this mutant still retains a residual Cu translocating activity (20 to 70% of WT ATP7B protein), most likely sufficient to prevent the disease only if the protein is correctly localized to the TGN (59-61). Moreover, ATP7B-H1069Q does not accumulate in transfected cells as its WT counterpart, suggesting a faster turn-over (62).

The mutation alters the structure of the nucleotide binding domain (NBD) (62), conferring thermal instability to the protein and thus preventing it from passing the quality control checkpoints in the ER. Little is known about ATP7B oligomerization. However, studies suggest that this process does occur since the 3rd and 4th Cu-binding domains in the N-terminal portion of ATP7B aggregate *in vitro* (63). In particular, because the H1069Q mutation may affect the strength of interaction between the NBD and N-terminal domains, the 3rd and 4th Cu-binding domains are able to oligomerize and generate ATP7B-H1069Q aggregates.

Taken together, these data suggest that the correction of the trafficking and localization of ATP7B-H1069Q should allow a substantial recovery of normal Cu metabolism. This finding offers a potential therapeutic application especially if the correction is applied in the late onset of the disease (at the age of 10-13 years) (64) before the manifestation of serious liver damage.

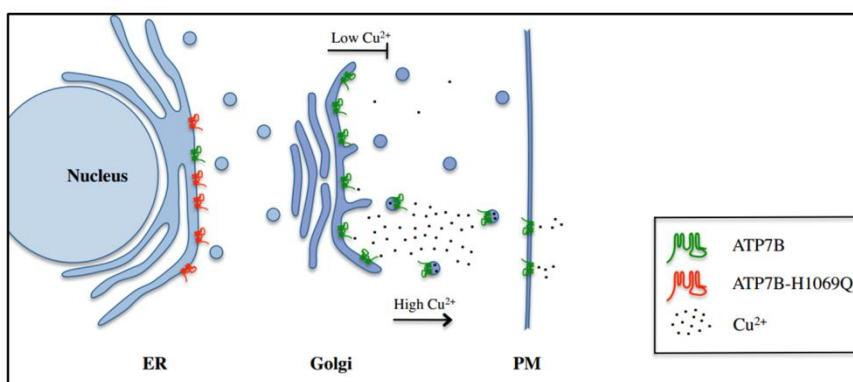


Fig. 5. Intracellular trafficking of ATP7B and ATP7B-H1069Q mutant in the presence of low or high Cu concentration.

1.5 Multifunctional cellular properties of α B-crystallin protein

The cellular chaperones are specialized proteins that not only help the nascent chains to attain native state (65-67), but also play a crucial role in the degradation and trafficking pathways. Moreover, the current view is that synthesis, folding, degradation and trafficking are strictly coordinated pathways that form the proteostasis network (68, 69). The rationale behind targeting chaperones in conformational diseases is that the overexpression (or repression) of the chaperone(s) most directly involved with a specific client protein might favourably induce homeostatic changes.

Indeed, a previous work has shown that the cytosolic chaperone α B-crystallin (CRYAB or sHSP-B5) plays a central role in correcting/preventing improper aggregation, thereby rescuing folding of ATP7B-H1069Q and Frizzled4-L501fsX533 (70).

In particular, α -crystallin, the major protein in the lens, consists of two subunits, α A (HspB4) and α B (HspB5), which possess nearly 55% sequence homology between them (71). It belongs to the family of small heat shock proteins and contains a core “ α -crystallin domain” (ACD). This domain is approximately 90 amino acids in length and is flanked by a variable hydrophobic N-terminal domain and a hydrophilic C-terminal domain (72) (Fig. 6). Both α A and α B are polydisperse oligomeric proteins, and their oligomeric size depends on their environment (73). α -crystallin represents approximately 40% of the protein in the human lens, where it exerts both a structural and functional role, with the α A and α B subunits present in approximately a 3:1 molar ratio (74).

α -crystallin is also present in other tissues. Predominantly present in the lens, low levels of α A are also expressed in the retina, thymus, and spleen (75, 76). Instead, α B-crystallin is present in relatively large quantities in the retina, skeletal muscles, kidneys, and heart (77, 78).

Being a member of sHSPs, CRYAB (175 aa) exhibits molecular chaperone-like activity, called holdase activity (henceforth referred to as chaperone); more specifically, it binds to structurally perturbed proteins, preventing their aggregation in an ATP-independent manner (79).

Besides its anti-aggregation activity, α -crystallins inhibit apoptosis induced by various factors. For example, in the lens epithelial cells, α -crystallins inhibit UVA-induced apoptosis through the regulation of PKC α , RAF/MEK/ERK, and AKT signaling pathways (80). In particular, α B-crystallin has also been shown to inhibit cytochrome c release from mitochondria and the downregulation of Bcl-2 in H₂O₂-treated cells (81). CRYAB is also involved in other cellular functions such as cell cycle, differentiation, gene expression, interaction with proteasome, and prevention of cytoskeleton destabilization (Fig. 7). Intriguingly, recent reports have

shown that CRYAB is also secreted by a non-conventional secretory pathway, suggesting a protective function also outside the cell (82). Several mutations are associated with CRYAB. For example, the R120G mutation, identified in 1998, causes the loss of chaperone function and the formation of protein precipitates inside cells (83). Malfunctions of CRYAB are associated with myopathy, neuropathy, ischemia, cataract, and cancer (84).

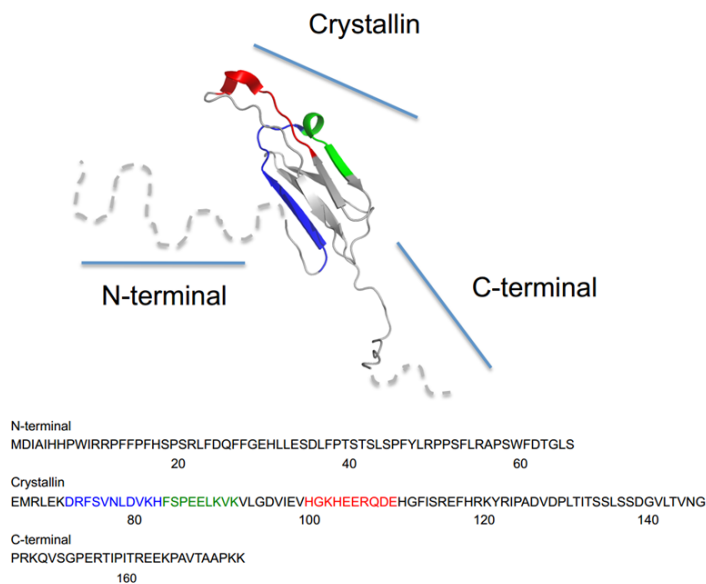
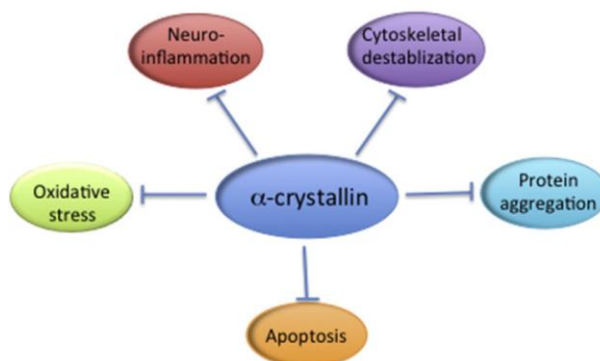


Fig. 6. Structural model of CRYAB protein and primary sequence of the 3 domains of CRYAB. Dashed line, region of the protein for which no crystallographic data are available. The N-terminal, crystallin and C-terminal extension domains are indicated. In the crystalline domain, the 3 major peptides endowed of chaperone activity in vitro (73-85, 73-92 and 101-110) are indicated in blue, blue + green, and red, respectively.



(Nagaray et al., 2015)

Fig. 7. α -crystallin inhibits several disease-contributing processes.

1.6 Phosphorylation modulates both the structural and functional properties of CRYAB

CRYAB exerts a variety of functions that most likely rely upon structural and functional changes, largely depending on post translational modifications (85). In particular, a major role in CRYAB function is played by phosphorylation occurring at 3 serine residues at positions 19, 45, and 59 of the N-terminal domain (86, 87). In fact, phosphorylation finely regulates CRYAB chaperone activity with multipass transmembrane proteins.

In particular, our previous work reported the effect of CRYAB phosphorylation on ATP7B-H1069Q and FZ4-FEVR receptor in transfected cells (88). In FZ4-FEVR mutant, a frameshift mutation (L501fsX533) generates a shorter C-terminal cytosolic tail of the receptor that accumulates in the ER of transfected cells, thereby blocking it from reaching the plasma membrane as FZ4 wild-type (89). Through a site directed mutagenesis strategy to substitute 3 relevant serine residues with aspartic acid, it is possible to mimic serine phosphorylation (90). The substitution with alanine residues in the same positions can prevent phosphorylation and is used to produce other types of mutants: the single and double pseudo-phosphorylated mutants.

The main results of my research project indicate that mimicking phosphorylation of serine 19 and 45, either singularly or in combination, causes loss of CRYAB chaperone activity, whereas the single phosphomimetic S59 has no such effect. On the other hand, pseudo-phosphorylation on serine 59 prevents the 19/45 phosphorylation-dependent inhibitory effect. However, this protecting effect is lost when all 3 serine

residues are simultaneously pseudo-phosphorylated. Moreover, the inhibition of chaperone activity does not correlate with the reduction of the oligomerization state of CRYAB, suggesting a direct role of phosphorylation in modulating both the structure and the function of the protein (88).

1.7 CRYAB-derived peptide: therapeutic perspectives for conformational diseases

Experimental demonstration of the beneficial effects of CRYAB clearly opens exciting therapeutic perspectives for several diseases of protein aggregation. However, its systemic administration has limitations owing to the specificity of action, rapid clearance of the protein, targeted delivery, and off-target effects.

Even more exciting has been the discovery that small peptides of both CRYAB and CRYAA also exhibit chaperone and anti-apoptotic activities. These peptides show remarkably similar activities to the whole protein. Furthermore, unlike the whole protein, peptides are easier to produce and are more amenable to manipulations for improvements in delivery and activities (79).

In particular, studies *in vitro* have demonstrated that isolated CRYAB derived peptides corresponding to residues 73-85 and 101-110 of the crystallin domain have anti-fibril formation activity (91), and that peptide 73-92 prevents aggregation and precipitation of denaturing alcohol dehydrogenase (92) (Fig. 6).

Most intriguingly, peptide 73-92 enters human fetal retinal pigment cells in culture via the sodium-coupled oligopeptide transporters 1 and 2 and protects them from apoptosis induced by oxidative stress. Even better protective results have been obtained with nanoparticles-containing peptides that are taken up by the cells (93). Moreover, this peptide, which enters via a lipid transporter, protects CHO and human lens pigment cells from thermal-stress induced apoptosis. Remarkably, intraperitoneal injection of the peptide inhibits cataract development in selenite-treated rats. In particular, the injected peptide reaches the lenses and inhibits oxidative stress, protein insolubilization, and caspase activity (94).

Although it remains to be formally proven that the CRYAB-derived peptide acts with the same mechanism as its full-length counterpart overexpressed in cells by transfection (70), much evidence supports the view that the peptide does mimic the effect of the full-length protein in all the parameters analyzed in different studies. In addition, evidence shows that the peptide has a

surprising ability to enter cells and to cross the blood aqueous barrier (93, 94).

Thus, these findings strongly sustain the exciting hypothesis that a CRYAB-derived peptide can effectively function as the full-length chaperone in live cells to restore ATP7B-H1069Q function.

1.8 Wilson disease models

The molecular mechanisms underlying WD associated with H1069Q mutation have not yet been confirmed in a proper H1069Q cell system. Indeed, although human hepatocytes remain the gold standard for the molecular analysis of WD in the liver, they do not represent a realistic option owing to the scarce number of cells in a biopsy and their inability to proliferate *in vitro*.

Lower eukaryotic models, like *ccc2* yeast, and the widely studied mammalian cell line, Chinese Hamster Ovary (CHO) cells, lacking ATP7B expression, represent useful systems to study the properties of ATP7B mutants. However, the problem with these cellular lines is that differences in species and organ source make it difficult for scientists to translate the results into human liver. On the other hand, human hepatoma cell lines are excellent cellular platforms to study ATP7B and its activity in Cu homeostasis, as indicated by the most commonly used hepatic cell line, Hep-G2. However, the fact that Hep-G2 and Huh-7, another human hepatic cell line, express endogenous and functional ATP7B may indeed hamper the study of the role of H1069Q mutation (95). Therefore, the use of heterologous or hepatoma-derived cell lines in which the mutant is overexpressed has obvious limitations owing to different genetic landscapes and proteostatic networks.

This obstacle could be circumvented by adopting a mammalian model for this form of WD, but unfortunately no such model has yet been generated. Recently, H/Q substitution has been achieved in *drosophila* ATP7 (dATP7). However, a major issue of this system is that insects do not have livers and dATP7 functions resemble those of mammalian ATP7A rather than those of ATP7B. In fact, dATP7 suppression leads to a severe Cu deficiency similar to Menkes phenotype in humans. Moreover, this system fails to recapitulate human disease because of genetic and epigenetic variability.

Therefore, the generation of cellular systems that would bear close similarities to patient-derived cells represents one of the most interesting therapeutic approaches to investigate the molecular features of H1069Q mutation and to screen disease-correcting strategies.

2. AIM OF THE THESIS

In this thesis, I will discuss the identification of new therapeutic perspectives for the most frequent ATP7B mutation causing Wilson Disease (WD). In particular, I will address the two pivotal aims of my PhD project: 1) the identification and exploitation of active peptides for therapeutic purposes in WD; 2) the generation of an isogenic cell model based on iPSCs obtained from skin fibroblasts of a homozygous WD patient and his mother, used as control, and their differentiation in hepatocyte-like cells (HLCs).

Regarding the first aim, in an attempt to find new and more efficient treatments for WD patients, we explored the pharmacologically active peptides present in cells overexpressing the H1069Q mutation of ATP7B. Such line of research was inspired by insightful evidence demonstrating that ATP7B-H1069Q retains a residual Cu transport activity despite being incapable of reaching its physiological destination and having an impaired Cu-dependent trafficking, due to its mislocalization in the ER. Therefore, evidence that α B-crystallin activity rescues localization and trafficking in response to Cu overload in ATP7B-H1069Q transfected cells generated our great interest in investigating the therapeutic potential of smaller portions of α B-crystallin. In particular, we examined peptide 73-92 for its anti-aggregation and anti-apoptotic activities *in vitro*, in cultured cell, and experimental animals.

To assess the beneficial effects of the synthetic peptide 73-92, we tested it in COS-7 cells transfected with GFP-ATP7B WT or mutant and in a stable human Hep-G2 KO cell line for the expression of ATP7B infected with an adenovirus carrying the previously mentioned constructs.

Regarding the second aim, we endeavored to create a cellular system that would allow us to delve deeper into the molecular dynamics responsible for the pathogenesis caused by ATP7B-H1069Q. Thus, to this end, we generated an isogenic cell model-based on iPSCs obtained from skin fibroblasts of a homozygous patient and his mother, used as control, and differentiated them into HLCs. Indeed, the novelty of our work lies in having shifted from the commonly used heterologous or hepatoma-derived cell lines overexpressing the mutant to a cellular model that would much more closely resemble a WD patient with isogenic expression of ATP7B-H1069Q. Remarkably, this new cell model gave us the opportunity to circumvent the use of cellular systems bearing a proteostatic network different from patient-derived cells, as well to overcome the limitations of hepatocytes from liver biopsies due to their scarce availability and inability to proliferate *in vitro*.

3. MATERIALS AND METHODS

cDNA cloning and plasmid construction

cDNA encoding CRYAB (ID: NM_001885.1) cloned into pCMV6-XL5 vector plasmid was obtained from Origene. To obtain the construct 3xFLAG-CRYAB, the cDNA coding for CRYAB was amplified from pCMV6-XL5 plasmid by PCR using the following oligos containing HindIII/XbaI flanking restriction sites and cloned into p3xFLAG-CMV-7.1:

- Fw (HindIII): 59-AAGCTTATGGACATCGCCATCCACCACCC-39;
- Rv (XbaI): 59-TCTAGACTATTTCTTGGGGGCTGCGG-39.

To obtain the construct 3xFLAG-CRYAB (R120G) in which the R120 was substituted with a glycine (G), the construct 3xFLAG-CRYAB was used as a template and site direct mutagenesis was performed according to the manufacturer instructions (Roche) using the following oligos:

- Fw: 59-CTCCAGGGAGTTCCACGGGAAATACCGGATCCCAG-39;
- Rv: 59-GTGGAACTCCCTGGAGATGAAACC-39.

To obtain the construct HA-CRYAB, the cDNA coding for CRYAB was amplified from pCMV6-XL5 plasmid by PCR using the following oligos containing HindIII/XbaI flanking restriction sites and cloned into pCDNA3 expression vector (Invitrogen):

- Fw (EcoRI): 59-GAATTCATGGACATCGCCATCCACCACCC-39;
- Rv (XhoI): 59-CTCGAGCTATTTCTTGGGGGCTGCGG-39.

DNA of ATP7B and ATP7B-H1069Q GFP-tagged at the N-terminus was provided by Svetlana Lutsenko (John Hopkins Medical School, Baltimore, MD) and by Dominik Huster (Otto-von-Guericke-University, Magdeburg, Germany).

Cloning strategy to generate HA-tagged CRYAB domains

The representative scheme of cloning strategy used in this study is shown in Fig. 8.

N-terminal, α -crystallin, and C-terminal domains were amplified using the Expand High Fidelity PCR System (Roche) and specific primers:

N-terminal domain

FW: 5'-GAATTCATGGACATCGCCATCCACC-3'

REV: 5'-CTCGAGCTATGAGAGAGTCCAGTGTCAAACC-3'

α -crystallin domain

FW: 5'-GAATTCCTCTCAGAGATGCGCCTGG-3'

REV: 5'-CTCGAGCTAATTCACAGTGAGGACCC-3'

C-terminal domain

FW: 5'-GAATTCCCAAGGAAACAGGTCTCTG-3'

REV: 5'-CTCGAGCTATTTCTTGGGGGCTGC-3'

The forward primers contain the restriction enzyme EcoRI recognition site, while the reverse primers contain the restriction enzyme XhoI recognition site. In the reverse primers used for the amplification of N-terminal and α -crystallin domains is also present a stop codon. Restriction enzymes EcoRI and XhoI recognition sites are compatible with the multiple cloning sites on the HAN(I)-pcDNA3 expression vector. The amplified gene was cloned into pCR 2.1-TOPO cloning vector (Invitrogen) and transformed into TOP10 Escherichia coli (E. coli) cells. Transformed cells were selected on a LB (Luria-Bertani) plate containing 100 μ g/mL ampicillin at 37°C for 16-18 h. Positive transformants were inoculated into LB broth containing 100 μ g/mL ampicillin for plasmid propagation. Plasmid was isolated and the presence of the DNA fragment of interest was determined by restriction enzyme digestion and DNA sequencing. The TOPO vector containing the DNA fragment of interest and the expression vector were then digested with the same enzymes (EcoRI and XhoI) to generate the same sticky ends. The digestion products of both the DNA of interest and the expression vector were ligated at room temperature for 5 min using the Rapid DNA Ligation Kit (Roche). Ligated mixture was transformed into TOP10 E. coli cells selected with the same strategies as those described above.

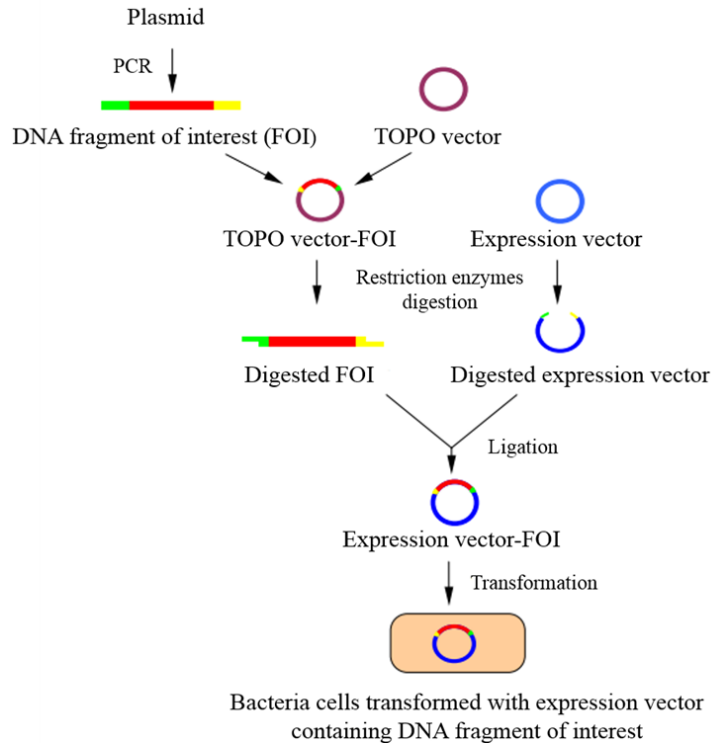


Fig. 8. Overview of gene cloning. FOI was amplified using gene specific primers incorporated with restriction enzyme digestion sites. The PCR product was cloned into pCR-2.1 TOPO vector. The gene was digested from the TOPO vector and ligated into an expression vector that was similarly digested. The ligated mixture was then transformed into an appropriate bacteria expression strain.

Cell culture

Cell lines were maintained in 5% CO₂ at 37°C in a humidified chamber. COS-7 (monkey kidney fibroblast-like cells) cell line was routinely grown in Dulbecco's modified essential medium (DMEM), containing 10% fetal bovine serum (FBS) and supplemented with 1% L-Glutamine and 1% penicillin/streptomycin.

Hep-G2 (human hepatocellular carcinoma) ATP7B knock-out cells, kindly provided by Roman Polishchuk, were cultured in Roswell Park Memorial Institute (RPMI) medium (Lonza) containing 10% fetal bovine serum (FBS) and supplemented with 1% L-Glutamine and 1% penicillin/streptomycin. ATP7B knockout was achieved by ZFN directed mutagenesis using Chandok *et al*'s method (95).

Transfection

COS-7 cells were cultured on coverslips in a 12-multiwell plate and, after 24 h, were transfected with X-tremeGene HP (Roche, Milan, Italy), according to the manufacturer's instructions, and using a 2:1 X-treme:DNA ratio.

Viral transduction

Hep-G2 KO cells were cultured on coverslips in a 24-multiwell plate, and, after 24 h, were infected with an adenovirus carrying GFP-ATP7B-H1069Q using a MOI= 700. Human adenovirus type 5 (dE1/E3) was produced by Vector Biolabs in HEK 293 as packaging cells and CMV promoter drives the expression of GFP-ATP7B-H1069Q.

Peptide treatment

CRYAB peptide (Pept1) and control peptides (inverted and scrambled sequence, respectively) were first chemically synthesized by GL Biochem (Shanghai, China) and then resuspended in H₂O to obtain a final concentration of 5 mM each. Synthetic peptides were either labeled or unlabeled with TAMRA to the side chain of amino group of Lysine residues at the carboxy or amino terminal ends. In all the experiments performed, 12.5 μM of each peptide was dissolved in a solution, composed of sterile water (25%) and culture medium (75%), and then added to the cells.

Immunofluorescence

COS-7 or Hep-G2 KO cells were seeded on coverslips. After 48 h from transfection or infection and after 24 h from treatment with 12.5 μM of both TAMRA-labeled or unlabeled Pept1 or Ctrl Pept, cells were fixed in PBS 1x-formaldehyde 3.7% for 30 min at room temperature and washed with PBS 1x. Then, they were permeabilized with 0.1% Triton-PBS 1x, treated with PBS 1x-BSA 1% for 15 min, and newly washed with PBS 1x. After that, they were subjected to indirect immunofluorescence staining.

Thus, the cells were incubated for 1 h at room temperature with the following primary antibodies: mouse monoclonal anti-FLAG (1:2000, Sigma), mouse monoclonal anti-HA (1:2000, Sigma), rabbit anti-GOLGA 2 (1:100, Sigma), and mouse monoclonal anti-LAMP1 (1:200, DSHB). Next they were washed with PBS 1x 3 times and incubated with the corresponding secondary

antibodies conjugated with Alexa Fluor 488, Alexa Fluor 568, and Alexa Fluor 633 (1:400, Life Technologies) for 45 min at room temperature. They were occasionally stained with Dapi (1:500, Sigma) and mounted in Mowiol. Finally, they were visualized with a 63x Plan-Apo/1.4 NA Oil lens using LSM510 Meta.

MTT assay

COS-7 cells or Hep-G2 KO cells were seeded in 96-well plates for 24 h and then exposed to 12.5 μ M of Pept1 or Ctrl Pept. During the peptide treatment, 10 μ l of 5 mg/ml MTT solution was added to each well for 4 h at 37°C. After removal of the medium, 100 μ l of 0.1 M HCl in Isopropanol was added to each well to dissolve formazan crystals. The absorbance at 570 nm was determined using the SYNERGY H1 microplate reader (Bio-Tek Instruments, Inc, Winooski, VT, USA).

Differential centrifugation

COS-7 cells were plated in p60 dishes. After 24 h, cells at 80% confluence were treated with TAMRA-labeled Pept1 or Ctrl Pept. After 20 h, the cells were resuspended in lysis buffer (10 mM Tris-HCl pH 7.4, 150 mM NaCl, 1 mM EDTA pH 8.0, and protease inhibitors 1x), incubated 30 min on ice and then lysed by sonication (2 pulses of 3 seconds; intensity: 2). The samples were then centrifuged at 16.000xg at 4°C for 30 min, the pellets (P16) resuspended in lysis buffer, and the supernatants centrifuged at 100.000xg at 4°C for 30 min (S100). Finally, the pellets (P100) were resuspended in lysis buffer (supplemented with 1% Triton). All the pellets and the supernatants obtained from the 100.000xg centrifugation were analyzed by spectrofluorimeter. The main phases of subcellular fractionation are described in Fig. 9.

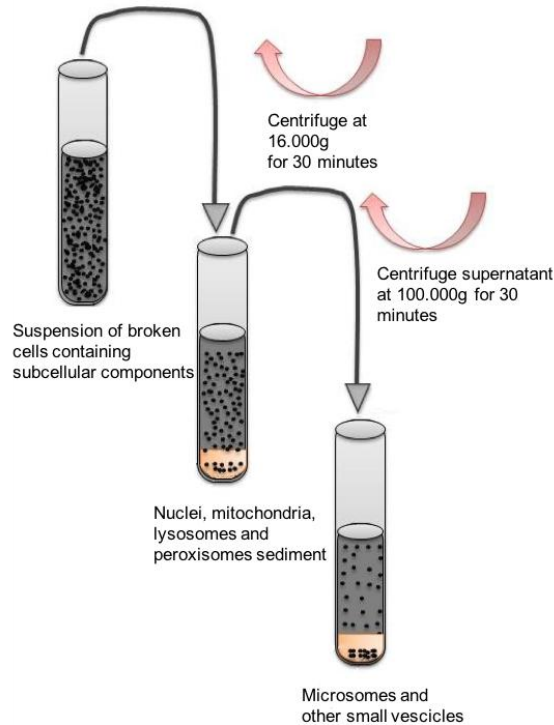


Fig. 9. Generation of P16, S100, and P100 subcellular fractions by differential centrifugation.

Copper treatment

COS-7 cells, seeded on coverslips in 12-multiwell plates, were transfected with pEGFP-C1-ATP7B WT or pEGFP-C1-ATP7B-H1069Q and treated with Pept1 or Ctrl Pept. After 48 h, the culture medium was changed to a fresh one containing either 200 μ M of CuSO_4 or 500 μ M of BCS. After 2 h, cells were subjected to indirect immunofluorescence procedure as above. Single confocal images were acquired at 63X magnification on a LSM510 Meta confocal microscope (Carl Zeiss, Jena, Germany).

FLIM-FRET

COS-7 cells were cultured on coverslips in 12-multiwell plates. After 24 h, cells were transfected with pEGFP-C1-ATP7B WT or pEGFP-C1-ATP7B-H1069Q as above. Twenty-four hours after transfection, the cells were treated with 12.5 μ M of both TAMRA-Pept1 or TAMRA-Ctrl Pept; Then, 48 h post transfection, cells were fixed with paraformaldehyde (2%) for 20 min. For FLIM-FRET analysis, TCS SMD SP5 Leica microscope equipped with FLIM module was used.

iPSC generation and differentiation

To obtain primary fibroblasts (authorization # 271/16 of the Ethical Committee of the University of Naples Federico II), skin biopsies from a patient and the healthy control (patient's mother) were cut (1 mm x 3 mm) into small pieces using a scalpel blade and cultivated on cell culture dishes in fibroblast medium consisting of DMEM supplemented with 20% FBS, 2 mM L-glutamine, and 1% penicillin and streptomycin (all from Invitrogen).

To generate iPSCs, 1×10^6 fibroblasts were transfected with a total of 1 μ g of each of the following episomal plasmids: pCXLE-hOCT3/4-shp53-F, pCXLE-hSK, pCXLE-hUL (all from Addgene) (96). Electroporation was carried out using a Nucleofector™ 2b Device (Lonza) by employing NHDF Nucleofector Kit (Lonza), following the manufacturer's instructions. Four days later, cells were plated on mitomycin inactivated fibroblasts (feeder) and cultivated in hES medium as follows: KO-DMEM, 20% Knock-out serum replacement (KOSR), 1x Glutamax, 1x μ M nonessential amino acids, 50 U/ml (penicillin and 50 mg/ml streptomycin), 100 μ M 2-mercaptoethanol (all from Invitrogen), and 10 ng ml⁻¹ bFGF (Peprotech). After 20-22 days, individual iPSC colonies were isolated and expanded for multiple passages (>5) on Matrigel (BD Biosciences) in mTeSR medium (Stem cell technologies) to remove feeder layer.

Generation of HLCs from iPSCs

To generate hepatocytes from both control and patient iPSC clones, we employed an already described method that allows efficient production of HLCs (97). Briefly, iPSC clones were plated on Matrigel and cultivated for 20-22 days. During this culture period, the medium composition was changed as follows: 5 days in RPMI media supplemented with B27 and 100ng/ml of Activin A (R&D), 5 days in RPMI media supplemented with

20ng/ml BMP4 (R&D) and 10ng/ml bFGF (Preprotech), 5 days in RPMI-B27 supplemented with 20ng/ml hepatocyte growth factor (HGF, Invitrogen) and finally further 5-7 days in hepatocyte culture medium (Lonza) supplemented with 20ng/ml oncostatin M (Invitrogen).

Immunofluorescence of control and patient iPSCs and HLCs

hiPSCs were fixed in 4% paraformaldehyde and permeabilized with 0.2% TX-100 in 10% FBS/1% BSA in 1x PBS for 7 min at room temperature; non-specific signals were blocked in 10% FBS/1% BSA in 1x PBS for 30 min at room temperature. Thus, the cells were incubated with primary antibodies in 10% FBS/1% BSA in 1x PBS overnight at 4°C. The primary antibodies used were the following: anti-Oct4 (1:500, Santa Cruz), anti-Nanog (1:500, Cell Signaling), anti- alpha-fetoprotein (1:400, Abcam), and anti-albumin (1:100, Dako). Following primary antibody incubation and washes in 1x PBS, the cells were incubated with Alexa- Fluor 488 or 594 secondary antibodies (1:400, Molecular Probes) and nuclei were stained with Dapi (1:5000, Calbiochem). Cells were then visualized with a 20×/0.40 (dry lens) objective using an inverted microscope (DMI4000, Leica Microsystems) at room temperature in 1x PBS. The images were captured with a digital camera (DFC365 FX, Leica Microsystems) using LAS-AF software (Leica Microsystems).

Preparation of cell extracts, SDS-PAGE, and Western blot analysis

After 20 days of differentiation, HLCs from control and patient iPSCs were treated with or without 100 mM cycloheximide (Sigma) for the indicated time period. Cells were lysed with lysis buffer containing 10 mM Tris-HCl pH 7.4, 150 mM NaCl, 1 mM EDTA pH 8, 1% Triton X-100 supplemented with cock-tail protease inhibitors (Roche Diagnostics) and protein concentration was determined by Bradford assay (Bio-Rad). Denaturation and reduction of protein samples for SDS-PAGE were performed at 37°C for 30 min. For each sample, 50 ug of total protein was loaded into 8% SDS gel and blotting was performed using a 0.45 µm nitrocellulose membrane (GE Healthcare). The blots were blocked for 1 h with 5% non-fat dry milk prepared in TBST (10 mmol/L Tris (pH 8), 150 mmol/L NaCl, 0.1% Tween 20) and subsequently incubated with primary antibody for ATP7B (rabbit polyclonal, 1:5000, Abcam), actin (rabbit polyclonal, 1:1000, Sigma) or vinculin (mouse monoclonal, 1:1000, Santa Cruz) as a protein loading control, for 1 h at room temperature. Blots were washed with TBST 3 times

and further incubated for 1 hour with secondary antibodies HRP-conjugated goat anti-rabbit (Santa Cruz) and anti-mouse IgG (Santa Cruz). Bound antibodies were detected by the ECL system (Santa Cruz). Densitometric analysis was performed using ImageJ 1.47v software.

Confocal immunofluorescence analysis

Control and patient HLCs, seeded on m-slide 8 Well (Ibidi) chamber, were fixed in 4% paraformaldehyde for 20 min, washed in 1x PBS, and permeabilized with 0.1% TX-100 in 1x PBS for 6 min at room temperature. Non-specific signals were blocked in 10% FBS/1% BSA in 1x PBS (blocking solution) for 30 min at room temperature. The cells were then incubated for 1 h with the following primary antibodies: rabbit anti-ATP7B (1:100), rabbit anti-BCAP31 (1:100, Proteintech), mouse monoclonal anti-Golgin-97 (1:400, Invitrogen), mouse monoclonal anti-KDEL (1:200, Enzo Life Sciences), and mouse monoclonal anti-LAMP1 (1:200, DSHB). The cells were then washed 3 times in PBS and incubated with the corresponding secondary antibodies conjugated with either Alexa Fluor 488 or Alexa Fluor 568 (Life Technologies) for 45 min, occasionally stained with Dapi (Sigma-Aldrich). Cells were visualized with a 63x Plan-Apo/1.4 NA Oil lens using LSM510 Meta or LSM710 confocal microscopes.

4. RESULTS

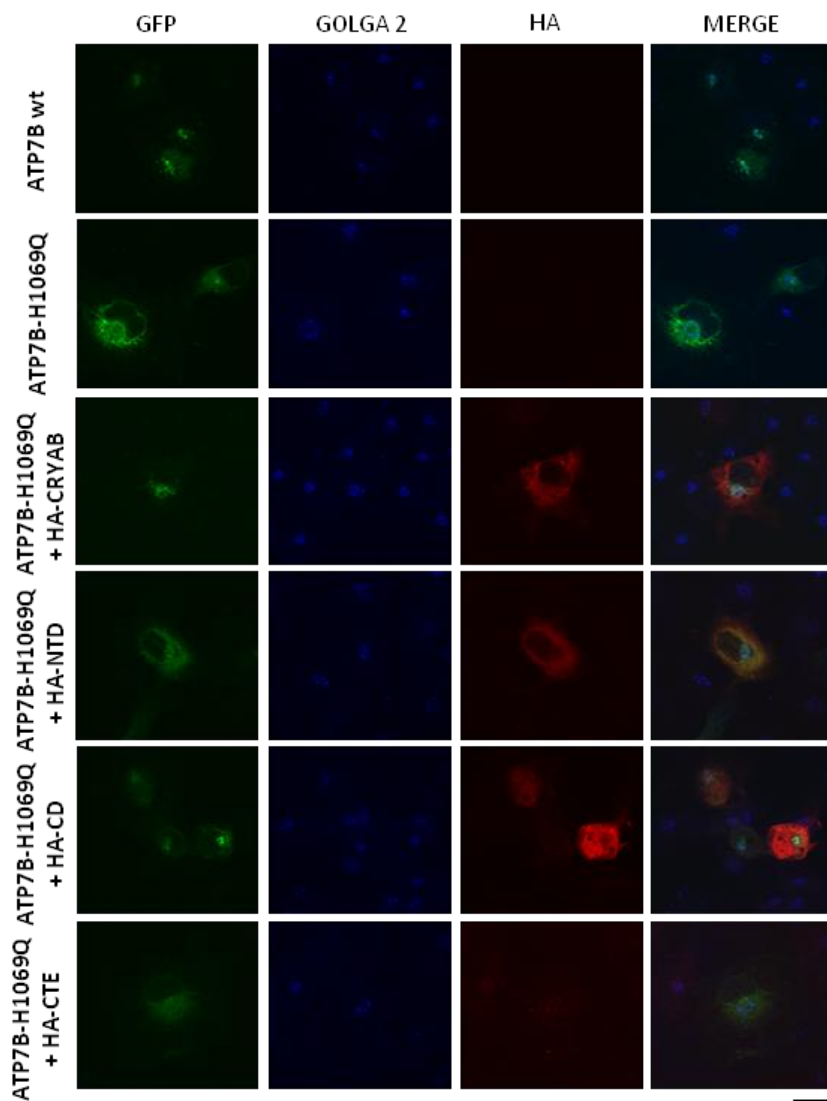
4.1 α -crystallin domain is able to rescue the physiological localization of ATP7B-H1069Q

Our results extend our recent findings demonstrating that CRYAB rescues ATP7B-H1069Q localization (70). A few years before that, another study had also demonstrated that isolated domains of CRYAB did maintain some level of chaperone activity *in vitro* (98). It is on the basis of this insightful evidence that we decided to explore even further whether a specific region of the whole protein could retain this functional role.

To explore this possibility, we dissected CRYAB in its main domains designing a suitable cloning strategy. In brief, the N-terminal (NTD) and α -crystallin (CD) domains, along with the C-terminal (CTE) extension (residues 1-66, 65-146, 148-175, respectively), were cloned in a HAN(I)pcDNA3 vector to generate HA-tagged polypeptides. Full-length CRYAB was cloned in the same vector. Each domain was functionally tested by co-transfecting COS-7 cells with ATP7B-H1069Q and its activity was compared to that of HA-CRYAB under the same cellular conditions. Transfection of ATP7B alone was used as positive control.

As demonstrated by confocal immunofluorescence analysis, no rescue effect occurred in the presence of the N-terminal and C-terminal constructs, as revealed by the reticular signal of ATP7B-H1069Q. In contrast, α -crystallin domain clearly mimicked the activity of the full-length protein, as confirmed by measuring the overlap of the GFP signal with GOLGA 2-blue staining (Golgi marker), calculated as Pearson's R value (Fig. 10).

Such finding strongly suggests that the α -crystallin domain retains the chaperone activity of the whole protein. Equally important, it also indicates the possibility of exploring the potential sequences in the α -crystallin domain that preserve these properties to test smaller molecules against the most frequent mutation causing Wilson disease.



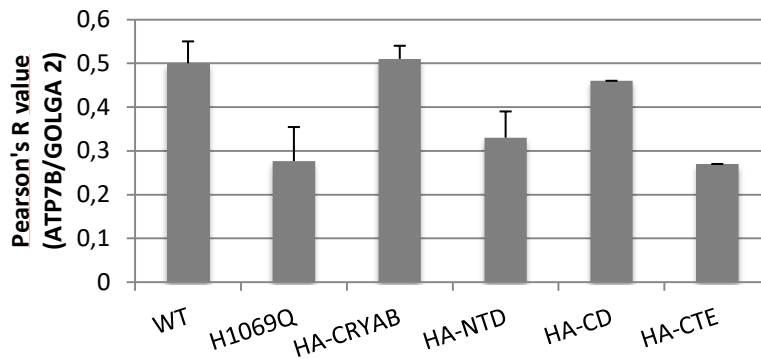


Fig. 10. α -crystallin domain corrects localization of ATP7B-H1069Q from the ER to the TGN. COS-7 cells were transfected to express GFP-tagged ATP7B or ATP7B-H1069Q and co-transfected with either HA-CRYAB or its domains (HA-NTD, HA-CD and HA-CTE respectively). Anti GOLGA 2 protein antibody was used to visualize the Golgi complex. The histogram below shows the percentage of ATP7B or ATP7B-H1069Q transfected cells exhibiting ER, Golgi, and ER plus Golgi staining (average \pm s.d., n=20 cells from 2 independent experiments). Scale bar: 10 μ m.

4.2 CRYAB-derived peptide does not affect cell viability

The discovery of mini-chaperones, *i.e.*, peptides derived from the α -crystallin chaperone region, has created new therapeutic perspectives to counteract diseases of protein aggregation (99). In particular, it has been previously reported that CRYAB peptide corresponding to residues 73-92 exhibits anti-aggregation and anti-apoptotic properties into cultured cells and in experimental animals (93, 94). Based on these findings, we used the synthetic peptide 73-92 (which we called Pept1) in our cellular models to investigate whether it could revert the WD phenotype as efficiently as the α -crystallin domain and the full-length protein. To verify the specificity of action, we used 2 control peptides with inverted and scrambled sequences. The peptides were labeled or unlabeled with TAMRA at the side chain amino group of the lysine residue at the C- or N- terminal ends (Fig. 11).

Our next step was then to test the toxicity of all peptides in 2 different cell lines: COS-7 and human Hep-G2 KO for ATP7B expression. Thus, we performed an MTT assay by incubating cells with 12.5 μ M of each peptide for 72, 96 and 120 h. We observed the peptides did not impair cell viability in

either cell line even after prolonged peptide exposure, compared to untreated cells (Fig. 12).

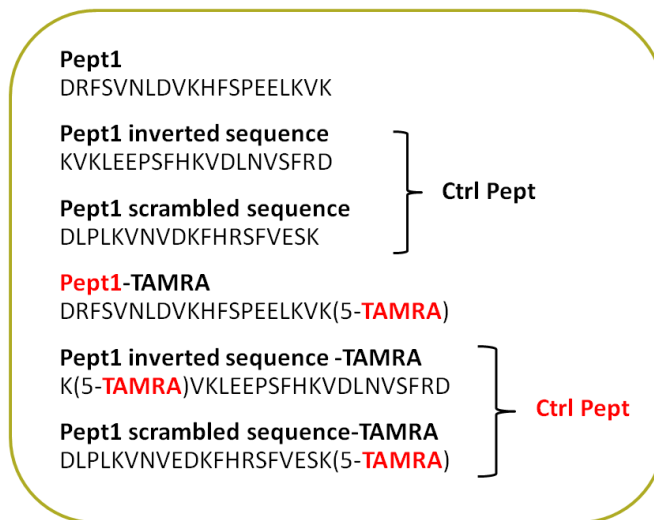


Fig. 11. Synthetic peptides used in the experimental plan. The box shows α B-crystallin-derived peptide sequence (Pept1) and the control peptides with inverted or scrambled sequence, labeled or unlabeled with TAMRA at the side chain amino group of Lys residue at the carboxy or the amino terminal ends.

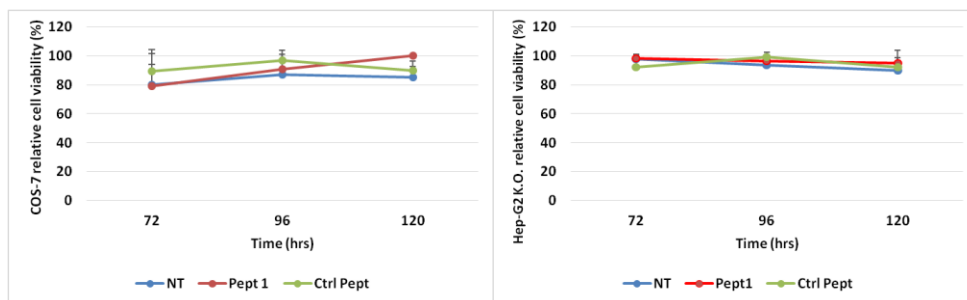


Fig. 12. Pept1 and Ctrl Pept do not impair cell survival. Cell viability of COS-7 and Hep-G2 KO cells was determined by MTT assay after 72, 96 and 120 h of peptide exposure. No significant differences were observed in the percentage of cell viability between cells incubated with Pept1 or Ctrl Pept and control. MTT data are represented as mean \pm s.d. of at least 3 independent experiments.

4.3 CRYAB peptide is mainly cytosolic and associated with vesicular compartments in a time-dependent manner

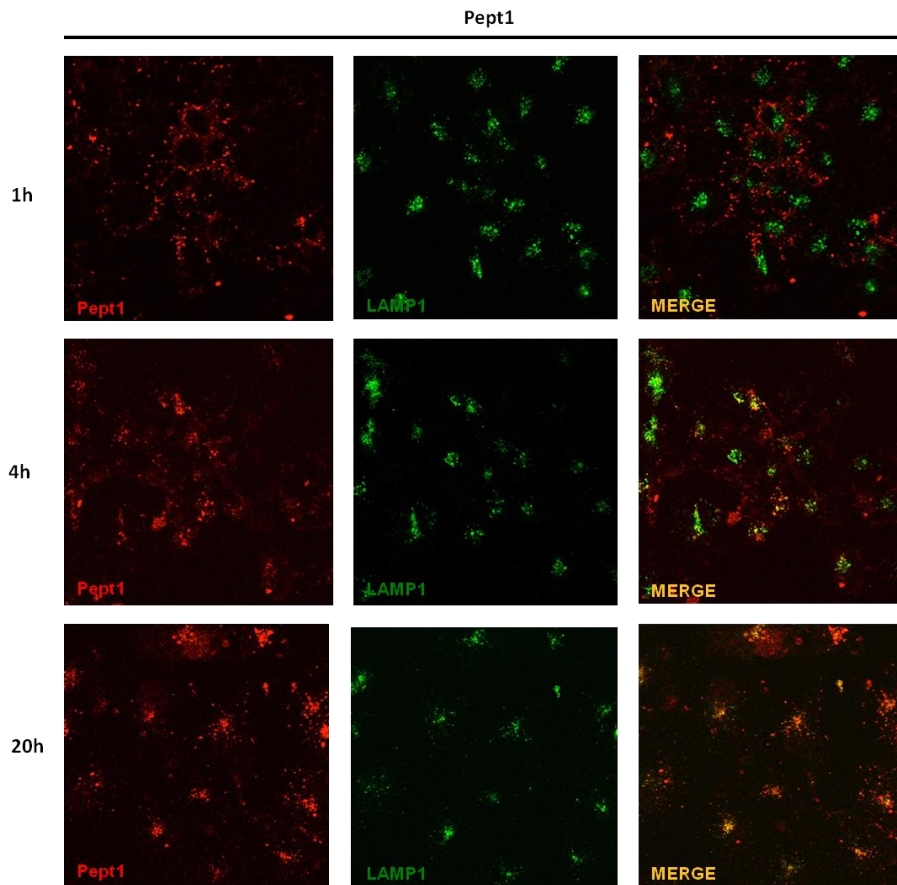
Since we found that both Pept1 and control peptide did not affect cell viability, we asked whether these peptides could be internalized by cells.

To verify this hypothesis, COS-7 cells were incubated with 12.5 μ M of TAMRA-labeled Pept1 and control peptide for 1, 4 and 20 h. An antibody against LAMP1 protein was used as a lysosomal marker.

Confocal immunofluorescence images showed that the peptide fluorescent signal was mainly cytosolic and partially colocalized with the lysosomal marker after 20 h (Fig. 13). This result strongly suggests that peptides are somehow able to enter COS-7 cells, albeit the entry mechanism remains unclear.

Furthermore, we fractionated, through differential centrifugation, COS-7 cellular extracts treated with TAMRA-conjugated peptides for 20 h. The subcellular fractions considered in the analysis were P16, S100, and P100. Fluorescence emission of each fraction was analysed by spectrofluorimetry. We found about 60% of peptide in the S100, confirming the immunofluorescence data about a cytosolic localization of the peptide. However, the presence of smaller amounts both in P16 and P100 fractions suggests an association of the peptide with vesicular compartments, as indicated by the colocalization with LAMP1 (Fig. 14). Overall, CRYAB

peptide enters the cells where it is mainly localized in the cytosol and partially in the vesicular structures in a time-dependent fashion.



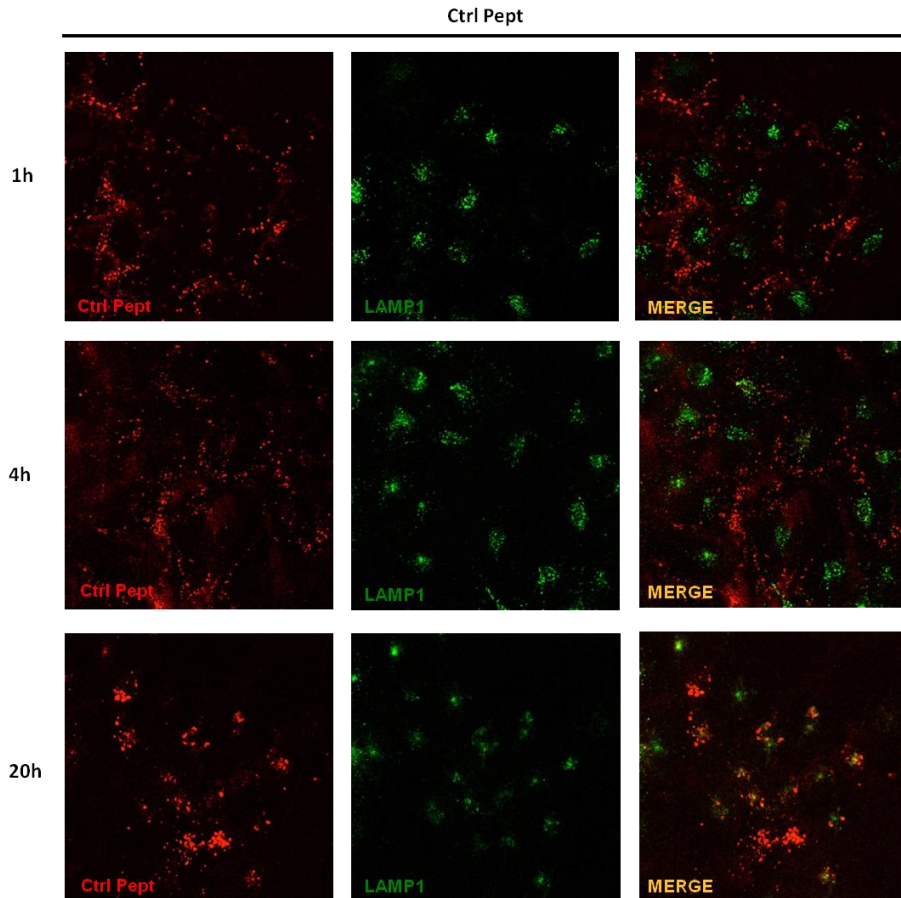


Fig. 13. CRYAB peptide and control peptide are internalized by COS-7 cells. COS-7 cells were incubated with 12.5 μM of TAMRA-labelled Pept1 and Ctrl Pept at the indicated times. Confocal immunofluorescence analysis was performed using an anti-LAMP1 protein antibody to visualize the lysosomes. Peptide fluorescent signal was evident in the cytosol after about 4 h and co-localization with LAMP1 was predominantly after 20 h. Scale bar: 10 μm .

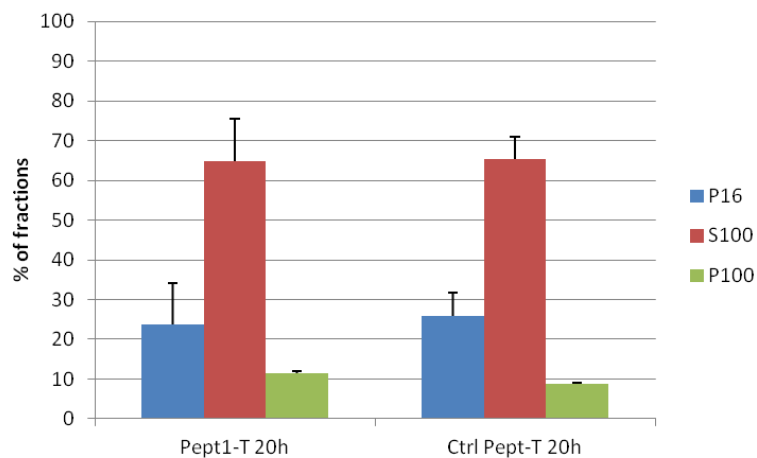
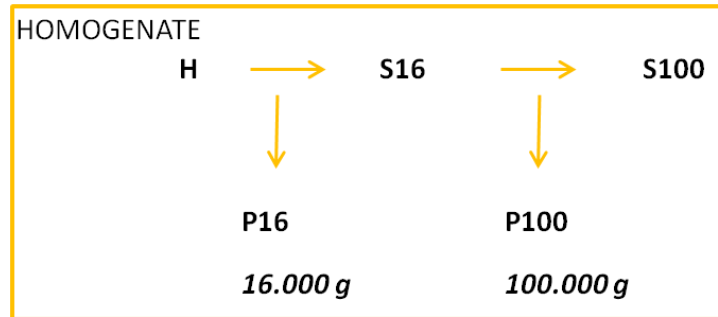


Fig. 14. CRYAB peptide localizes mainly in the cytosolic fraction of COS-7 cells. Cells were incubated with 12.5 μ M of TAMRA-labeled Pept1 and Ctrl Pept for 20 h, lysed, and then separated into subcellular fractions using variable centrifugation, as indicated in the scheme. Fluorescence emission of each fraction was determined by spectrofluorimeter and reported as percentage of P16, S100, P100 in the graph below.

4.4 Comparing the effect of CRYAB peptide on the localization of ATP7B-H1069Q in COS-7, Hep-G2 KO, and Huh-7 cell lines

COS-7 cells were transfected to express the GFP-tagged ATP7B localizing with GOLGA 2-blue staining (Golgi marker) or ATP7B-H1069Q whose signal was clearly reticular. Intriguingly, we found that in cells expressing ATP7B-H1069Q and co-transfected with full-length CRYAB or treated with 12.5 μ M of Pept1 (labeled or unlabeled with TAMRA) for 24 h, ATP7B-H1069Q was able to rescue the Golgi localization. No such effects were observed in the presence of either CRYAB-R120G or control peptide. Under both conditions, the mutant was mainly retained in the ER (Fig. 15).

This evidence was strongly supported by quantitative analysis of ATP7B or ATP7B-H1069Q transfected cells exhibiting ER, Golgi, or ER plus Golgi staining. In the presence of the CRYAB peptide, percentage of cells showing a Golgi signal of the mutant is prevalent and comparable to that of cells co-transfected with full-length CRYAB. Furthermore, we confirmed the rescue activity of Pept1 on the mutant by measuring the overlap of GFP signal with GOLGA 2-blue staining, calculated as Pearson's R value (Fig. 15).

In addition, although COS-7 cell line is easy to manipulate, we decided to perform the same experimental design in cellular models that would reflect much more closely the pathophysiology of a WD. In particular, we used Hep-G2 KO and Huh-7 because they are excellent cellular platforms to study Cu homeostasis (95). The reason we chose a stable human Hep-G2 KO cell line for ATP7B expression was to abolish the risk of endogenous expression of ATP7B (95). In brief, we performed the same experimental plan and peptide treatment conditions in Hep-G2 KO and Huh-7 (Tackling the Most Frequent Wilson Disease-Causing ATP7B Mutation: Mechanism of Rescue by α B-Crystallin and its Derived Peptide, Ph.D. Michela Ciano). However, Huh-7 were transfected with the same constructs used for COS-7 cells, whereas Hep-G2 KO were infected with an adenovirus carrying GFP-ATP7B-H1069Q given that viral infection considerably increases the population of cells expressing the mutant protein compared to the DNA transfection. Colocalization of GFP-ATP7B-H1069Q with the Golgi marker was generated as Pearson's R value.

As expected, confocal immunofluorescence and colocalization analysis (Fig. 16) in Hep-G2 KO fully confirmed those obtained in COS-7 cells and Huh-7 (data not shown). CRYAB peptide was able to correct the localization of the mutant, clearly suggesting the beneficial effects and the specificity of this peptide in different cellular disease models.

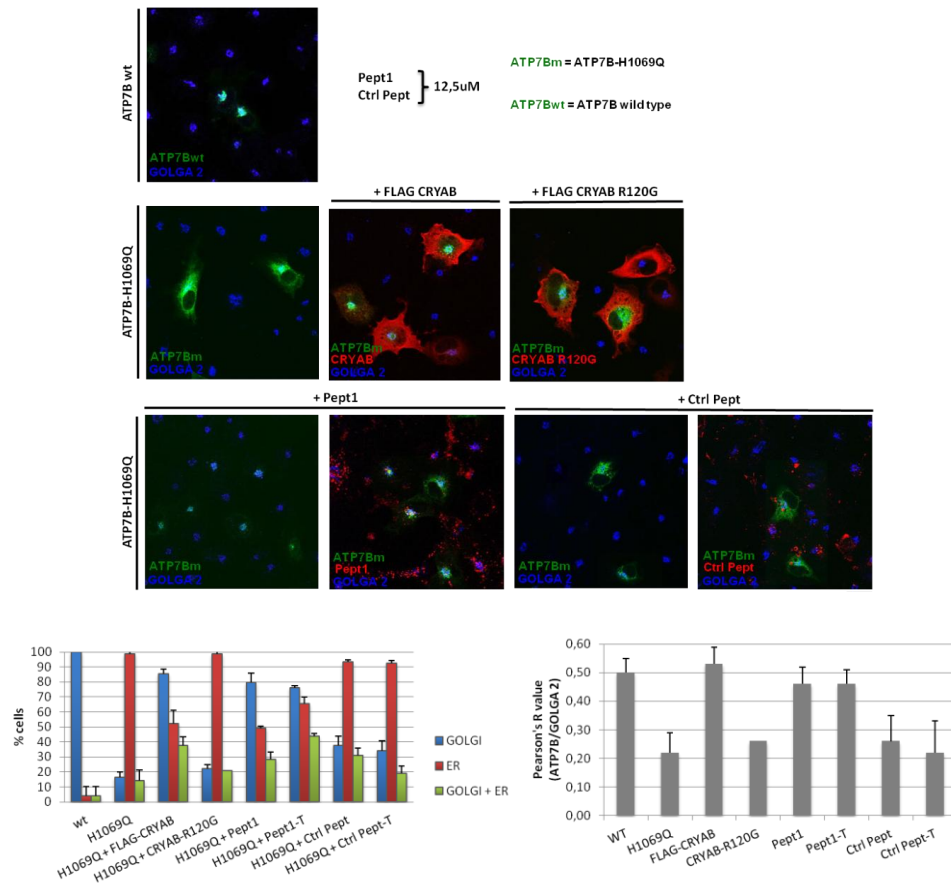
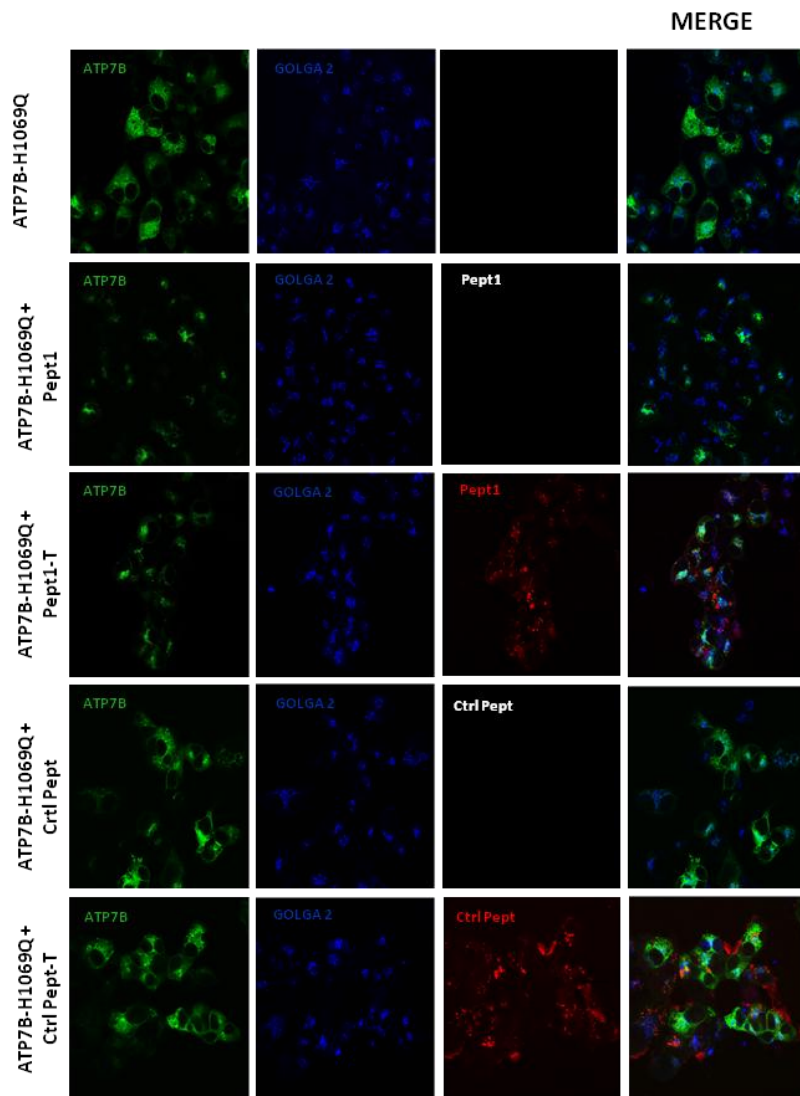


Fig. 15. Pept1 corrects localization of ATP7B-H1069Q from the ER to the Golgi complex. COS-7 cells were transfected to express GFP-tagged ATP7B or ATP7B-H1069Q and co-transfected with either 3xFlag-CRYAB or CRYAB-R120G or incubated with Pept1 and Ctrl Pept (12.5 μ M), in the presence or absence of TAMRA, for 24 h post-transfection. Subsequently, the cells were processed for confocal immunofluorescence analysis using an anti-GOLGA 2 protein antibody to visualize the Golgi complex. In the presence of full-length CRYAB or both forms of Pept1, ATP7B-H1069Q fluorescence signal mainly localized with the Golgi marker, whereas it was clearly reticular in the cells co-transfected with CRYAB-R120G or treated with Ctrl Pept. Scale bar: 10 μ m.

The histogram below shows the percentage of ATP7B or ATP7B-H1069Q transfected cells exhibiting ER, Golgi complex, and ER + Golgi complex staining (mean \pm s.d., n=25 cells from 2 independent experiments).

Colocalization of GFP and GOLGA 2 signals was determined with the ImageJ colocalization plugin and the obtained Pearson's R value is shown on the right.



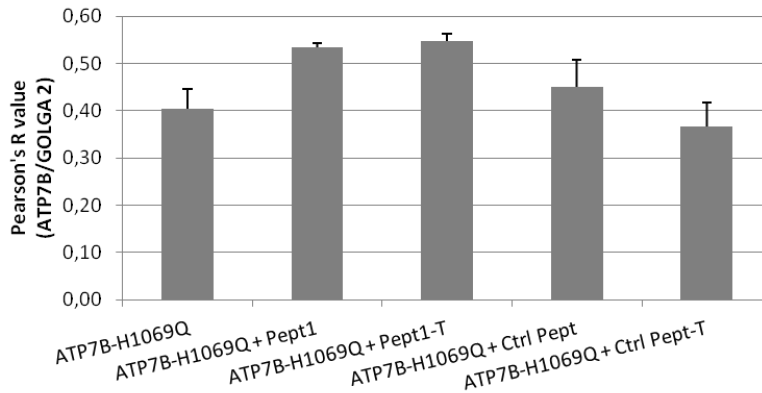


Fig. 16. Rescue activity of Pept1 on ATP7B mutant in Hep-G2 KO. Hep-G2 KO cells were infected with GFP-ATP7B-H1069Q. After 24 h, cells were treated with 12.5 μ M of either Pept1 or Ctrl Pept conjugated or unconjugated with TAMRA. In the presence of Pept1, ATP7B-H1069Q was rescued to the Golgi; instead, in the presence of Ctrl Pept, ATP7B-H1069Q was retained in the ER. Colocalization of GFP and GOLGA 2 signals was determined with the ImageJ colocalization plugin; the obtained Pearson's R value is shown on the right. Scale bar: 10 μ m.

4.5 Golgi-corrected ATP7B-H1069Q redistributes to post Golgi vesicles in response to copper overload

Another important issue was to investigate whether Pept1 could restore post-Golgi trafficking activity of the mutant in response to increased copper concentrations.

To address this question, we designed the same immunofluorescence experiment previously described in COS-7 cells. In brief, before fixation, cells were incubated for 2 h in a medium containing either 200 μ M of cupronic sulphate (CuSO_4) or 500 μ M of bathocuproine disulphonate (BCS), a copper chelator. Because ATP7B is able to move to LEs/lysosomes and PM in response to excess Cu (70), rescuing of Cu-dependent post-trafficking of the mutant was verified with ATP7B as positive control.

The cells treated with BCS showed an evident Golgi localization of both ATP7B and mutant transporter in the presence of CRYAB peptide (Fig. 17). Interestingly, only in the presence of Pept1, ATP7B-H1069Q changed the subcellular localization from perinuclear compartments to post-Golgi vesicles in response to copper excess, similarly to ATP7B. Consequently, we observed an increase in ATP7B-H1069Q transfected cells exhibiting Golgi

staining in the BCS condition and vesicular staining after copper treatment (Fig. 17).

In contrast, none of the described effects occurred with control peptide.

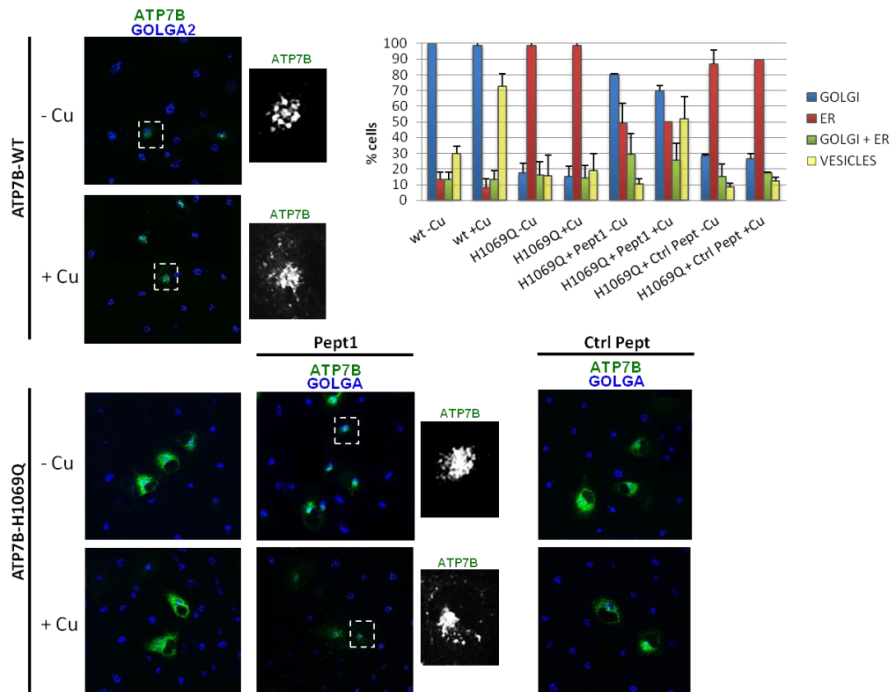


Fig. 17. The Golgi-corrected ATP7B-H1069Q moves to post-Golgi vesicles in response to Cu overload in the presence of Pept1. COS-7 cells were transfected with GFP-tagged ATP7B or ATP7B-H1069Q and either co-transfected with 3xFlag-CRYAB or CRYAB-R120G (data not shown) or incubated with Pept1 and Ctrl Pept (12.5 μ M) for 24 h post-transfection. Two days after transfection, cells were incubated for 2 h in a medium containing either 200 μ M CuSO₄ (+Cu) or 500 μ M of the Cu chelant BCS (bathocuproinedisulfonic acid) (-Cu), and subsequently processed for confocal immunofluorescence analysis using an anti-GOLGA 2 protein antibody to visualize the Golgi complex. The white spots indicate a Golgi localization of ATP7B and ATP7B-H1069Q in the presence of Pept1 using low Cu conditions, whereas a punctate staining pattern of ATP7B and ATP7B-H1069Q with Pept1 is dispersed through the cytosolic vesicular compartment upon Cu exposure. Scale bar: 10 μ m.

The histogram shows the percentage of ATP7B or ATP7B-H1069Q transfected cells exhibiting ER, Golgi complex, ER + Golgi complex, and PM + vesicular staining (average \pm s.d., n=25 cells from 2 independent experiments).

4.6 CRYAB peptide interacts with ATP7B-H1069Q

To elucidate the mechanism of action of Pept1, we investigated whether it interacted with the WT and/or the mutated form of ATP7B through a FLIM-FRET analysis and a co-immunoprecipitation (co-IP) assay followed by mass spectrometry (MS) analysis in COS-7 cells.

In particular, fluorescence resonance energy transfer (FRET) microscopy is a technique used for quantifying the distance between two different fluorophores. It involves the transfer of energy from a fluorescent donor in its excited state to another excitable fluorophore. Therefore, FRET occurs when 1) the distance between the donor and acceptor molecules is small (1-10 nm); 2) the fluorescence emission spectrum of the donor molecule overlaps (to some extent) the excitation spectrum of the acceptor; 3) the donor emission decreases while the acceptor emission increases. (100).

The principle of Fluorescence Lifetime Imaging Microscopy (FLIM) analysis is the same, except that it measures the donor fluorescence lifetime (τ), rather than the intensity of fluorophore signal.

The advantage of measuring fluorescence lifetime is that this parameter is directly dependent upon excited-state reactions but independent of fluorophore concentrations and the emission intensity through the sample, conditions difficult to take under control (101).

A FRET phenomenon causes the reduction of donor lifetime due to the energy transfer toward the acceptor molecule (Fig. 18). Thus, when FLIM is measured in the presence of FRET, the donor lifetime reduction proves the putative interaction between two molecules.

In our experimental plan, we transfected COS-7 cells with either GFP-ATP7B or GFP-ATP7B-H1069Q (GFP was used as donor molecule) and treated them with 12.5 μ M of TAMRA-labelled Pept1 or control peptide for 24 h (TAMRA was the acceptor fluorophore) (Fig. 18). FLIM-FRET analysis was performed in collaboration with Professor Sarnataro at CEINGE.

For FLIM analysis, we used a random population of cells. We found that only in CRYAB-treated cells exhibiting a Golgi-like phenotype of the mutant, the donor fluorescence lifetime (GFP) decreased meaningfully (Fig. 19). This result was emphasized by a 12% FRET efficiency value, calculated as percentage of the ratio between τ of donor with acceptor and τ of donor alone (Fig. 19). According to the literature data, this represents a significant value of FRET efficiency, suggesting a putative and preferential interaction between the CRYAB peptide and the mutated form of ATP7B. TAMRA-Ctrl Pept did not show a significant FRET signal, thereby providing evidence of a sequence-specific mechanism.

We also performed co-immunoprecipitation in COS-7 cells treated as described above. After cellular lysis, the cells were incubated with a primary

antibody anti-GFP and then with Protein A-Sepharose beads. The immunoprecipitated samples were analysed through selected ion monitoring mass spectrometry (SIM-MS) in collaboration with Professor's Scaloni group at ISPAAM (Michela Ciano Ph.D. thesis). This technique is particularly recommended when having to investigate the binding of small peptides given that it is highly sensitive for the detection and the identification of amino acids and peptides. The SIM-MS analysis confirmed the interaction between Pept1 and ATP7B-H1069Q, strongly supporting the FLIM-FRET data (data not shown).

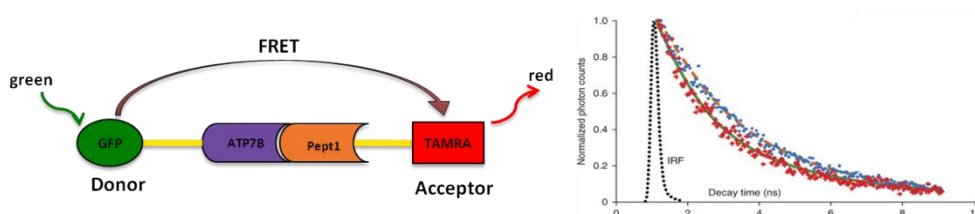


Fig. 18. Schematic representation of the principle of FLIM-FRET and fluorophores used in the experiment. The curve indicates the donor fluorescence lifetime (τ) that decreases when there is energy transfer towards the acceptor.

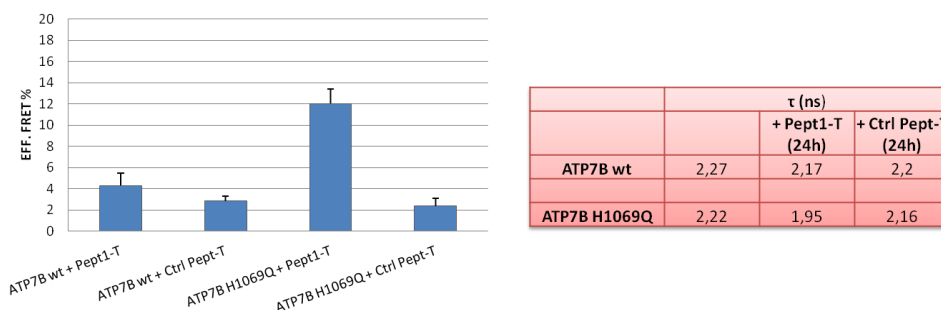


Fig. 19. Pept 1 interacts with ATP7B-H1069Q. COS-7 cells were transfected with GFP-tagged ATP7B or ATP7B-H1069Q and incubated with TAMRA-labeled Pept1 and Ctrl Pept (12.5 μ M) for 24 h post-transfection. Then, cells were processed for FLIM analysis. The lifetimes of GFP-tagged ATP7B and ATP7B-H1069Q alone or with TAMRA-labeled peptides are reported in the table on the right.

On the left, the histograms show the percentage of FRET efficiency. A value of 12% strongly indicates that FRET occurs between Pept1-T and GFP-ATP7B-H1069Q (average \pm s.d., at least 10 cells from 3 independent experiments).

4.7 Differentiation toward hepatocytes of iPSCs obtained by reprogramming skin fibroblasts from a WD patient and his mother (control)

All the studies discussed in the above sections were performed by overexpressing the mutant transporter in heterologous cells. However, we later realized that the only reliable strategy to study the molecular phenotype of the WD mutation and validate our *in vitro* results was to generate a new WD cellular system with the isogenic expression of the pathogenic mutant.

To this aim, we used primary fibroblasts from skin biopsies of a WD patient carrying the H1069Q mutation (H1069Q/H1069Q) and his mother, as control (WT/H1069Q) (henceforth indicated as patient and control) to generate induced pluripotent stem cells (iPSCs) (Fig. 20).

The generation, characterization, and hepatic differentiation of iPSCs was performed in collaboration with Doctor Silvia Parisi, Roman Polishchuk, Michela Ciano, and Anna Musto. iPSCs were generated using an integration-free method based on the transfection of episomal plasmids vectors into primary fibroblasts (96). Three weeks later, the iPSCs-like colonies were assessed for Nanog and Oct 4 stemness markers positivity by immunofluorescence (Fig. 21). After picking and expanding several clones from both samples, 2 WD iPSCs clones and 2 control iPSCs, which showed a normal karyotype, were grown under feeder-free conditions to avoid feeder contamination during differentiation. To ensure the maintenance of pluripotent stem cell markers, the expression of Oct 4 and Nanog was evaluated after multiple passages (≥ 15) through immunofluorescence microscopy and quantitative real-time RT-PCR (qPCR).

For our purposes, we differentiated patient and control iPSCs into hepatocyte-like cells (HLCs) (Fig. 20) using a previously established protocol (97). This protocol comprises 3 hepatic developmental stages: definitive endoderm, hepatic progenitors and hepatocyte-like cells. The appearance of markers representative of each phase was assessed by immunofluorescence microscopy and qPCR. The cells were differentiated for 20 days, the time span required to result positive for hepatic cell markers: albumin (ALB) (data not shown), α -fetoprotein (AFP), and α 1-antitrypsin (AAT) (Fig. 21). Importantly, there were no differences between control and patient HLCs in the expression of differentiation markers, suggesting that the ATP7B mutation does not affect hepatic differentiation in our conditions.

Finally, qPCR revealed a strong expression of ATP7B during hepatic differentiation; instead, immunofluorescence analysis showed that ATP7B positive population varied between 30 and 40% of the total cell population, similarly to control and patient HLCs (data not shown).

Thus, we advance the hypothesis that the generation of HCLs from control and patient iPSCs provides a powerful isogenic *in vitro* model to study ATP7B mutation.

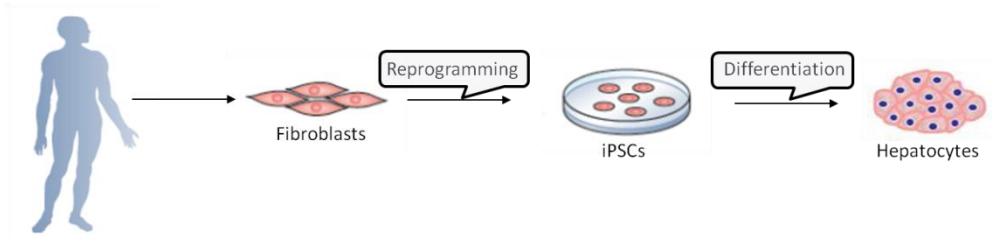


Fig. 20. Diagram of the main phases for the generation of a new isogenic WD cellular model.

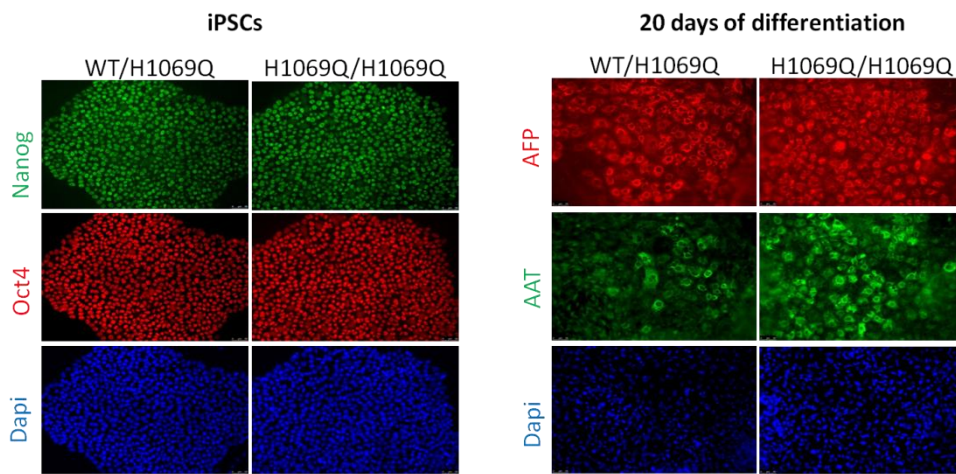


Fig. 21. Generation of iPSCs from human fibroblasts heterozygous and homozygous for the H1069Q mutation of ATP7B and characterization of HCLs obtained from iPSCs. Human fibroblasts from control (WT/H1069Q) and patient (H1069Q/H1069Q) were induced to reprogram; twenty-one days later, the presence of pluripotent stem cells colonies was assessed by immunofluorescence for stemness marker expression (Oct 4 and Nanog). The nuclei were stained with DAPI. Scale bars: 100 μ m.

The completion of hepatic differentiation was evaluated at 20 days by analyzing the presence of the functional hepatic marker AAT co-expressed with AFP. Scale bars: 50 μ m.

4.8 ATP7B shows both a reticular and Golgi localization and is degraded faster in patient HLCs than in control HLCs

Subcellular distribution of ATP7B was investigated through confocal immunofluorescence analysis. After fixation, the cells were double-labeled with an antibody against ATP7B and with either Golgin 97 to recognize the Golgi complex or KDEL, used as an ER marker.

In accordance with our experiments in heterologous and hepatic cell lines, we observed that in control HLCs ATP7B clearly colocalized with Golgin 97, indicating its Golgi localization.

However, a single most striking result emerged from these experiments. In brief, whereas in previous work we demonstrated that ATP7B-H1069Q resides almost exclusively in the ER and that only a very small fraction is able to reach the Golgi compartment, here we observed that in patient HLCs, a significant fluorescence signal of the mutant was in the Golgi, whereas only moderate levels of ATP7B-H1069Q were detectable in the ER, possibly owing to the rapid degradation of the mutant (Fig. 22).

Based on this result, we could speculate that, even though the mutation affects the trafficking of Cu transporter from the ER to Golgi, a significant part of the protein might nonetheless manage to pass the ER quality control checkpoints and reach the Golgi complex.

In collaboration with Doctor Michela Ciano, Elena Polishchuk, and Roman Polishchuk, we tested this hypothesis by comparing overall ATP7B quantities in control and patient HLCs using Western Blot analysis. No ATP7B expression was detected in undifferentiated iPSCs of control and patient. By contrast, whereas it was strongly expressed in HLCs derived from control iPSCs, the mutant was dimly expressed in HLCs derived from patient iPSCs (Fig. 23A).

Moreover, in the presence of cycloheximide (Chx), a protein synthesis inhibitor, a clear reduction in ATP7B-H1069Q level was observed after 4 h in patient HLCs, confirming the faster degradation of ATP7B-H1069Q compared to the WT protein (Fig. 23B).

We also performed immunofluorescence analysis after treating cells with MG132, a reversible proteasome inhibitor that acts at the final step of the ER-associated degradation (ERAD) pathway. A clear reticular signal of ATP7B mutant was visible in patient HLCs exposed to MG132, suggesting that mutant degradation is due to ER retention (Fig. 23C).

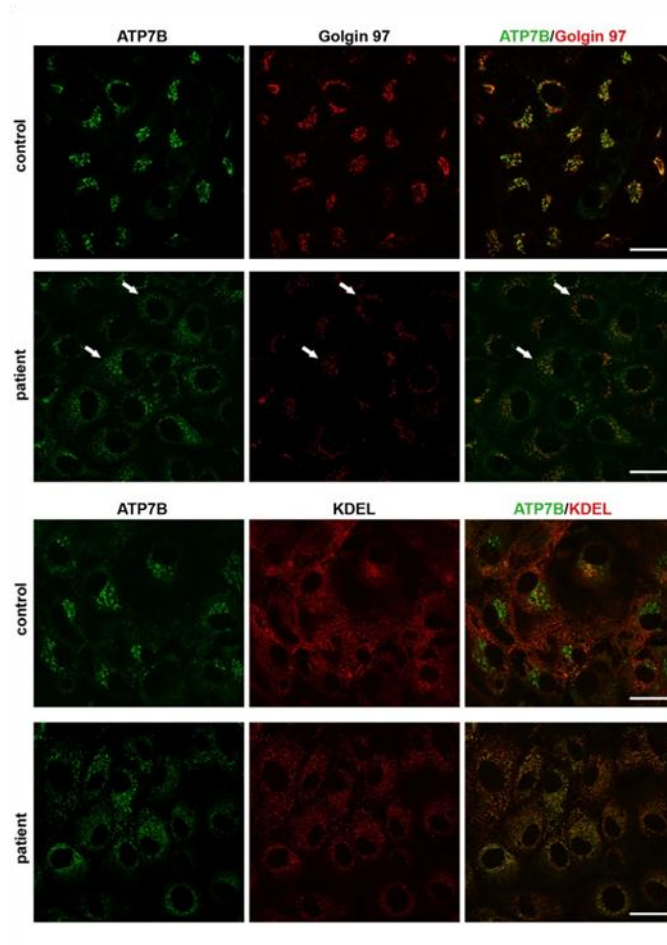


Fig. 22. Intracellular localization of ATP7B in HLCs obtained from control and patient iPSCs. Confocal immunofluorescence analysis of HLCs immunolabeled for ATP7B and Golgin 97 (upper panels) or KDEL containing proteins (lower panels) as markers of Golgi complex and ER, respectively. White arrows point to Golgi complex containing ATP7B-H1069Q in patient HLCs. Scale bars: 10 μ m.

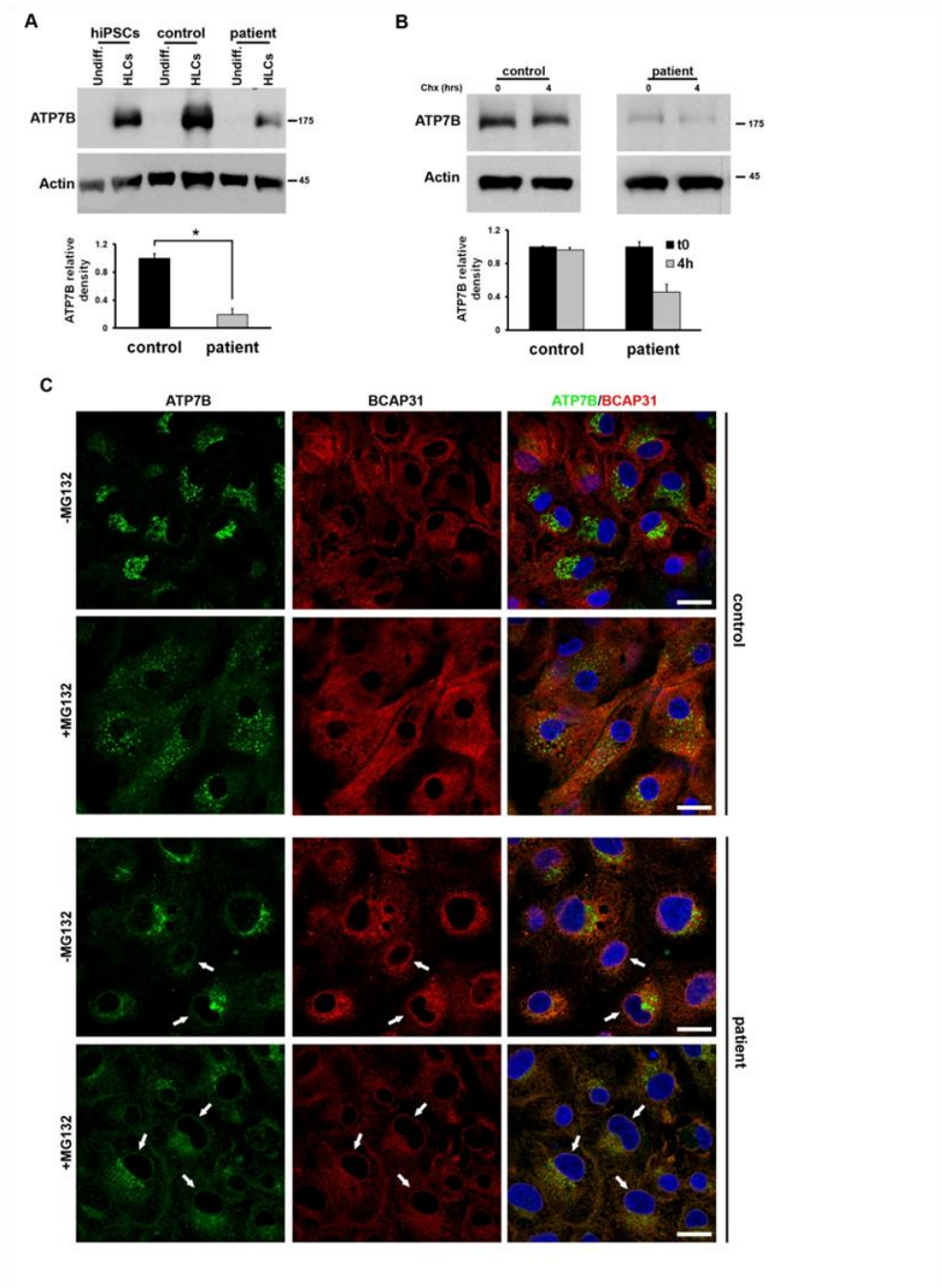


Fig. 23. Relative accumulation and degradation of ATP7B in HLCs obtained from control and patient iPSCs. (A) Western blot analysis of ATP7B accumulation at steady state in undifferentiated iPSCs and in the differentiated HLCs. Unrelated human iPSCs were used as further control.

The graph shows the relative expression of ATP7B in patient HLCs normalized to the level in the control HLCs. Data are reported as means \pm SEM of 3 biological replicates. (B) Western blot analysis of ATP7B accumulation in control and patient HLCs incubated for 4 h in the absence or in the presence of 100 μ M cycloheximide. The graph shows the relative expression of ATP7B at the 4 h time point normalized to the level of the 0 time point. Data are reported as means \pm SEM of 3 biological replicates. (C) Cells were treated with 30 μ M MG132 for 6 h, then fix labeled with antibodies against ATP7B and ER resident protein BCAP31. Arrows indicate the ER, where ATP7B colocalizes with BCAP31 in patient hepatocyte-like cells. Scale bars: 6 μ m.

4.9 Golgi ATP7B pool responds to increasing copper levels in patient HLCs

To better understand whether ATP7B-H1069Q retains its ability to redistribute to Cu excretion sites, we performed confocal immunofluorescence analysis after incubating cells with CuSO₄ for 2 h. As expected, in control cells ATP7B was able to relocate towards post Golgi structures containing the LE/lysosome marker LAMP1 in response to increasing Cu levels. Intriguingly, in patient HLCs, the Golgi ATP7B pool showed a similar redistribution in the presence of copper overload (Fig. 24). This result suggests that ATP7B-H1069Q isogenically expressed in patient HLCs preserves its trafficking response to Cu overload, a finding that represents an important step towards the characterization of a mutant rescue strategy.

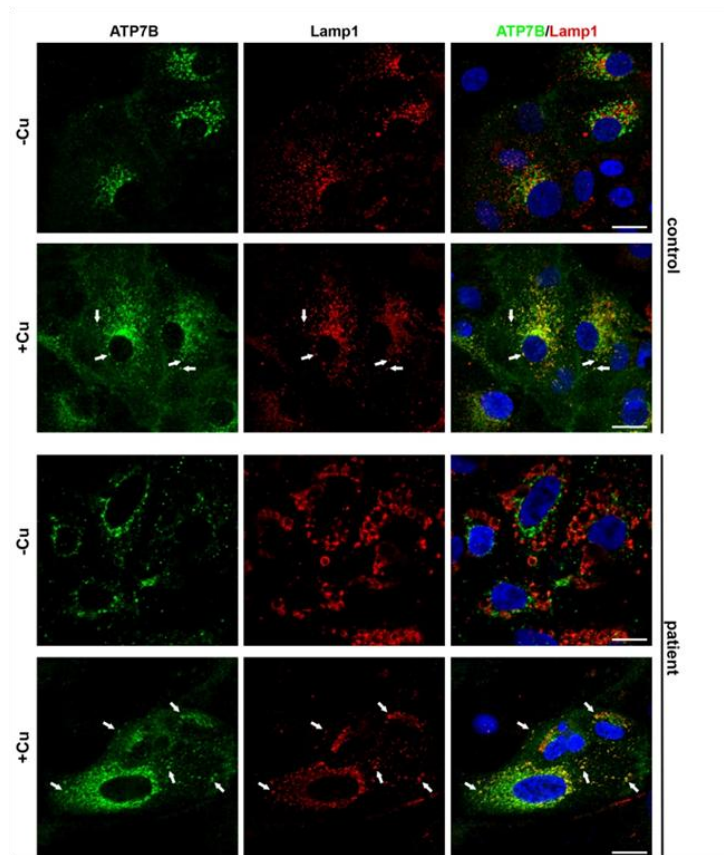


Fig. 24. Trafficking of ATP7B in response to high Cu level in HLCs obtained from control and patient iPSCs. Cells were treated with 200 μ M CuSO_4 for 2 h and double-labeled with antibodies against ATP7B and LAMP1. Arrows indicate LAMP1-positive structures containing ATP7B both in control and patient hepatocyte-like cells exposed to Cu. Scale bars: 5.7 μ m

5. CONCLUSIONS AND DISCUSSION

Wilson Disease is a rare, inherited autosomal recessive disorder affecting 1/7000 children worldwide (21). Prompt detection and early treatment are paramount to reverse its course. As of today, chelating agents and zinc therapy are considered the gold-standard treatments. The downside, however, is that despite being highly effective, they may give rise to serious adverse effects. Thus, the overall motivation of my research project was to identify new therapeutic prospects for the most frequent ATP7B mutation causing Wilson Disease. Extending on previous lines of research demonstrating that ATP7B-H1069 mutation retains residual Cu transport activity and that α B-crystallin may very well play a pivotal role in correcting the mutant's mislocalization to the ER, we set out to investigate the potential therapeutic implications of CRYAB-derived peptides in the treatment of WD. Moreover, to further corroborate our hypotheses and obtain more reliable results, we decided to step away from the more common heterologous or hepatoma-derived cell lines and generated an isogenic WD cell line based on iPSCs from skin fibroblasts of a WD patient and his mother (control) and differentiated them into HLCs.

Remarkably, some insightful findings emerged from my PhD project. First, we found that CRYAB-derived peptide (*viz*, 73-92) rescues the proper intracellular localization and Cu-dependent trafficking of ATP7B-H1069Q. Indeed, we demonstrated for the first time the beneficial effects of a mini-chaperone against the most frequent cause of Wilson disease in heterologous or hepatoma-derived cell lines overexpressing the mutant protein.

Second, we succeeded in generating a new isogenic WD cell model derived from iPSCs obtained by reprogramming fibroblasts from a patient and his mother, used as control. Thanks to the efficiency of this model, we were able to characterize for the first time the molecular dynamics of endogenously expressed ATP7B-H1069Q. The most important finding emerging under isogenic conditions was that loss of ATP7B function is mainly due to the rapid ER-associated degradation of the mutant, whereas only part of ATP7B-H1069Q survives and localizes to the trans-Golgi compartment. Noteworthy, this result challenges the conventional view of ATP7B-H1069Q overexpression studies reporting that a massive accumulation of the mutant is caused by its inability to pass the ER control quality checkpoints.

Properties of CRYAB-derived peptide in cells overexpressing ATP7B-H1069Q

Wilson disease caused by ATP7B-H1069Q is thought to be caused by a partial misfolding of the protein. Consequently, stabilization of the native protein represents a logical therapeutic approach to ameliorate the pathological consequences (99).

To reach this goal, cellular chaperones constitute the most obvious target. The rationale of targeting chaperones in conformational diseases is that modulating the expression level of the chaperone(s) most directly involved with a specific client protein might favorably induce homeostatic changes. Besides anti-aggregation properties, chaperones also participate in degradation and trafficking processes. Such pathways are closely intertwined with protein synthesis and folding, constituting the cellular proteostasis network (68, 69). Several studies have already demonstrated the multifunctional cellular properties of chaperones in diseases associated with protein aggregation and apoptosis (93, 94). In particular, α A- and α B-crystallins have been studied extensively for their multiple functions in the lens where they are mainly expressed and in other tissues, and for their well recognized chaperone-like function (102).

In a previous work, we demonstrated that the full-length CRYAB protein rescues the localization and trafficking of ATP7B-H1069Q in response to copper overload in transfected cells (70). This represented a very promising result to tackle the disease. However, the use of a full-length chaperone for therapeutic purposes has obvious limitations owing to the molecular size and specificity of action. Indeed, each chaperone has multiple sites of interaction with different client proteins (93), thus modulating its expression could translate into impairing the proteostasis network of the cell. To overcome these obstacles, we dissected the whole protein in its main domains. Our analysis clearly indicated that the α -crystallin domain retains chaperone activity, whereas the N-terminal and C-terminal domains fail to mimic the effect of the parent protein in cells overexpressing the ATP7B mutant. This result fueled our interest in exploring the potential sequences in the crystallin domain of CRYAB able to retain a rescuing activity toward ATP7B-H1069Q. In this context, studies *in vitro* have shown that isolated peptides corresponding to residues 73-85 and 101-110 of the crystallin domain prevent fibril formation activity (91), whereas peptide 73-92 prevents aggregation and precipitation of denaturing alcohol dehydrogenase (92).

The demonstration of chaperone-like activities in peptides derived from a smaller portion of the α -crystallin domain clearly suggests the possibility of exploiting these mini-chaperones as a very effective therapeutic molecule (99). Indeed, unlike the parental protein, these peptides are smaller and more

amenable to manipulations for improvements in delivery, availability, target specificity, and molecular activities (79). Most relevant for these purposes is CRYAB-derived peptide 73-92. Recent studies have indeed demonstrated that this peptide exhibits anti-aggregation and anti-apoptotic effects in both cultured cells and experimental animals exposed to stress conditions (93, 94). Given its therapeutic potential, we have tested the synthetic CRYAB-derived peptide (73-92) in heterologous or hepatoma-derived cell lines overexpressing ATP7B-H1069Q to see if it was able to counteract Cu toxicity. For our purposes, we also used a form conjugated with TAMRA to track its intracellular localization.

Remarkably, our experiments indicated that the peptide enters the cells and does not affect cell viability even after prolonged incubation periods. Although we still do not know how it actually penetrates into cells, our subcellular fractionation studies revealed that the peptide is mainly cytosolic and is only partially associated with lysosomes structures in a time-dependent fashion. Thus, the peptide exhibits important non toxicity properties and a cytosolic distribution most likely functional to its activity.

The investigation of its role in the context of H1069Q mutation produced the most interesting results. First, we found that in the presence of the CRYAB peptide, ATP7B-H1069Q was rescued and correctly localized to the Golgi compartment. Moreover, the Golgi corrected ATP7B-H1069Q was also able to redistribute to post Golgi sites and, eventually, to the PM, in cells treated with the peptide and exposed to high Cu level.

The ability of the peptide to rescue the Cu-dependent trafficking raised many questions about its mechanism of action. A first indication came from our FLIM-FRET and SIMS analysis. These analyses revealed that the CRYAB peptide interacts with the ATP7B copper transporter. Although many more questions remain unanswered, this finding does represent a first step towards understanding the mechanism of action against ATP7B-H1069Q mutant.

Taken together these results open new promising avenues for correcting the the most frequent ATP7B mutation causing Wilson disease. Undoubtedly, an extensive biochemical and structural characterization of the peptide would provide a powerful instrument to identify the crucial residues and best possible modifications aimed at improving the activity of the peptide. In this context, CRYAB peptide could be used as a guide for high-throughput screenings to identify already druggable small molecules apt to correct the mislocalization of ATP7B-H1069Q. Finally, the study of its mechanism of action could expand our understanding of protein folding and open new therapeutic possibilities for Wilson disease and beyond.

New isogenic WD cell model and characterization of endogenously expressed ATP7B-H1069Q

Validating disease-correcting strategies in cellular systems that would bear close similarities to patient-derived cells represents one of the most interesting therapeutic perspectives for protein-misfolding-mistrafficking diseases. Accordingly, one of the main research achievements in my PhD project has been the creation of a cellular model based on the differentiation of iPSCs into hepatocyte-like cells (HLCs). These cells were obtained by reprogramming skin fibroblasts of a homozygous (H1069Q/H1069Q) patient, and his mother, the latter used as control (WT/H1069Q). Thus, we obtained HLCs expressing the endogenous ATP7B forms at physiological level in the proper genetic background.

In fact, previous studies have reported the generation of iPSCs from WD patients with R778L and M769V genetic mutations of ATP7B (**103**, **104**). However, to our knowledge, we are the first research team to have generated human iPSCs from patients bearing the H1069Q ATP7B mutation. Moreover, two other aspects characterizing our cellular model are worthy of attention: 1) the use of episomal plasmids instead of retro- or lentivirus for reprogramming induction to avoid genetic integration in the patient's cells; 2) the choice of a familiar control instead of human ESCs derived from human embryo of unrelated individuals, as described in other studies.

From a future perspective, this model will offer scientists the opportunity to overcome the limitations of heterologous cellular systems that exhibit different genetic landscapes and proteostatic networks. One could argue that this obstacle could be circumvented by adopting a mammalian model. However, one drawback of using this system is that it could fail to recapitulate human disease because of genetic and epigenetic variability, thereby undermining drug validation screenings (**105**). Still another option could be the use of hepatocytes from liver biopsies. However, a disadvantage of this approach is the scant availability of cells from biopsies and their inability to proliferate *in vitro* (**106**). A more valid option for drug validation purpose could be the use of skin fibroblasts. Indeed, unlike other types of cell lines, they can be easily manipulated and expanded *in vitro*. In the context of ATP7B mutation, however, skin fibroblasts do not represent a valid alternative because they do not express ATP7B at a detectable level.

All things considered, our HLC model system provides an excellent solution to test mutant-correcting strategies in WD and to overcome all the intrinsic limitations of other cellular models.

Practically, HLCs offer several advantages. They are of human origin, have hepatocyte features, endogenously express the ATP7B-H1069Q mutant, and, finally, can be abundantly differentiated from iPSCs. Still another major

advantage is that iPSCs can also be differentiated into neurons. This additional property could enable researchers to study this mutation in the brain, considering that the H1069Q mutation of ATP7B is frequently associated with neurological aberration (107). Moreover, applying the recent CRISPR/Cas9 editing technology on patients' iPSCs could generate WT/H1069Q, WT/WT, and null/null iPSCs a strategy that could throw more light on the complex dynamics of this mutant.

The generation of this new WD cellular model has allowed us to study, for the first time, the molecular dynamics of ATP7B-H1069Q under isogenic conditions.

The main finding emerging from our experiments is that loss of ATP7B function is mainly due to a higher degradation of the misfolded protein.

Another surprising finding of my research is that a significant pool of the mutant protein is present in the Golgi compartment, a finding that challenges previous studies reporting a strong accumulation of ATP7B-H1069Q in the ER. Moreover, the overall amount of ATP7B protein in patient HLCs was 3 times lower than that in control cells, although ATP7B mRNA levels were similar. Taken together these results suggest that although most of the newly-synthesized mutant undergoes rapid degradation, a small part of ATP7B-H1069Q survives, thereby reaching the Golgi destination.

In this regard, we have also demonstrated that the rapid degradation of the mutant takes place in the ER. Indeed, the suppression of proteasomal degradation strongly increases ATP7B mutant signal in the ER of patient HLCs. We also observed that the fraction of the mutant in the TGN is able to move to LEs/lysosomes structures in response to increased levels of Cu, as efficiently as the WT transporter. This is in line with the results obtained in the presence of CRYAB peptide. Unfortunately, this Cu-dependent trafficking response is not sufficient to prevent the disease because of the decreased expression of ATP7B-H1069Q. Therefore, new therapeutic research aimed at increasing the number of molecules reaching the TGN is highly warranted.

In contrast, the results of our studies as well as those of others, performed by overexpressing ATP7B-H1069Q in heterologous or hepatoma-derived cell lines, have indicated that ATP7B-H1069Q is massively trapped in the ER, exhibiting a severely impaired trafficking capability to Golgi and ER/lysosome structures in response to Cu overload (45, 58, 59, 70, 108). Regardless of such ER retention, the mutant conserves a significant residual Cu transport activity tantamount to 20 to 70% of WT ATP7B protein (59, 61). Such evidence has led to the conclusion that treatments that facilitate the sorting of the mutant from the ER into the secretory pathway would represent a major therapeutic approach. However, evidence that ATP7B-H1069Q undergoes an accelerated ER-associated degradation would also seem to

suggest that using inhibitors to reduce the mutant's rapid degradation could be a crucially valid alternative to counter WD-associated ATP7B-H1069Q mutant.

Unquestionably, the major findings emerging from my research project do warrant further investigation. Accordingly, future studies will need (1) to further optimize our new isogenic model system, for instance, by increasing the population of HLCs obtained after iPSCs differentiation, (2) they will need to validate the rescuing activity of CRYAB peptide, and (3) they will need to test the safety and efficiency of other correcting agents for this common form of WD. However, I am adamantly hopeful that my research team, also thanks to the fruitful collaboration with other research labs, has laid the groundwork for future efforts in this arduous but promising line of research.

6. ACKNOWLEDGEMENTS

This work was supported by Telethon grant n. GGP 14002 to S.B. I wish to thank Prof. Massimo Mallardo and Dr. Maria Gabriella Caporaso for their technical help and useful advices and Dr. Paola Merolla for editing the final draft of my thesis.

7. REFERENCES

- 1) **de Bie P, Muller P, Wijmenga C, Klom LWJ.** Molecular pathogenesis of Wilson and Menkes disease: correlation of mutations with molecular defects and disease phenotypes. *J Med Genet* 2007; 44:673-688.
- 2) **Lutsenko S, Barnes NL, Bartee MY, Dmitriev OY.** Function and Regulation of Human Copper-Transporting ATPases. *Physiol Rev* 2007; 87:1011-1046.
- 3) **Bissig K D, Honer M, Zimmermann K, Summer K H, Solioz M.** Whole animal copper flux assessed by positron emission tomography in the Long-Evans cinnamon rat-a feasibility study. *Biometals* 2005; 18:83-88.
- 4) **Linder MC, Moriya M, Whon A, Kassa A, Gilley C.** Vesicular transport of Fe and interaction with other metal ions in polarized Caco2 cell monolayers. *Biol Res* 2006; 39:143-156.
- 5) **Culotta VC, Yang M, O'Halloran TV.** Activation of superoxide dismutases: putting the metal to the pedal. *Biochim Biophys Acta* 2006; 1763:747-758.
- 6) **Horng YC, Cobine PA, Maxfield AB, Carr HS, Winge DR.** Specific copper transfer from the Cox17 metallochaperone to both Sco1 and Cox11 in the assembly of yeast cytochrome *c* oxidase. *J Biol Chem* 2004; 279:35334-35340.
- 7) **Prohaska JR, Gybina AA.** Intracellular copper transport in mammals. *J Nutr* 2004; 134:1003-1006.
- 8) **Punter FA, Glerum DM.** Mutagenesis reveals a specific role for Cox17p in copper transport to cytochrome oxidase. *J Biol Chem* 2003; 278:30875-30880.
- 9) **Hamza I, Faisst A, Prohaska J, Chen J, Gruss P, Gitlin JD.** The metallochaperone Atox1 plays a critical role in perinatal copper homeostasis. *Proc Natl Acad Sci USA* 2001; 98:6848-6852.

- 10) **Hamza I, Prohaska J, Gitlin JD.** Essential role for Atox1 in the copper-mediated intracellular trafficking of the Menkes ATPase. *Proc Natl Acad Sci USA* 2003; 100:1215-1220.
- 11) **Walker JM, Tsivkovskii R, Lutsenko S.** Metallochaperone Atox1 transfers copper to the NH₂-terminal domain of the Wilson's disease protein and regulates its catalytic activity. *J Biol Chem* 2002; 277:27953-27959.
- 12) **Menkes JH, Alter M, Steigleder GK, Weakley DR, Sung JH.** A sex-linked recessive disorder with retardation of growth, peculiar hair, and focal cerebral and cerebellar degeneration. *Pediatrics* 1962; 29:764-79.
- 13) **Danks DM, Campbell PE, Walker-Smith J, Stevens BJ, Gillespie JM, Blomfield J, Turner B.** Menkes' kinky-hair syndrome. *Lancet* 1972; 1:1100-2.
- 14) **Tonnesen T, Kleijer WJ, Horn N.** Incidence of Menkes disease. *Hum Genet* 1991; 86:408-10.
- 15) **Gu YH, Kodama H, Shiga K, Nakata S, Yanagawa Y, Ozawa H.** A survey of Japanese patients with Menkes disease from 1990 to 2003: incidence and early signs before typical symptomatic onset, pointing the way to earlier diagnosis. *J Inherit Metab Dis* 2005; 28:473-8.
- 16) **Danks DM.** Disorders of Copper transport. In: **Scriver CR, Beaudet AL, Sly WM, et al, eds.** *The metabolic and molecular basis of inherited disease.* New York: McGraw-Hill 1995; 2211-35.
- 17) **Kaler SG.** Diagnosis and therapy of Menkes syndrome, a genetic form of copper deficiency. *Am J Clin Nutr* 1998; 67:1029S-1034S.
- 18) **Kodama H, Murata Y.** Molecular genetics and pathophysiology of Menkes disease. *Pediatr Int* 1999; 41:430-435.
- 19) **Kodama H, Murata Y, Kobayashi M.** Clinical manifestations and treatment of Menkes disease and its variants. *Pediatr Int* 1999; 41:423-429.

- 20) **Fei W, Jing W, Chunwen P, Liang Q, and Chunmeng J.** Wilson's Disease: A Comprehensive Review of the Molecular Mechanisms. *Int J Mol Sci* 2015; 16, 6419-6431.
- 21) **Coffey AJ, Durkie M, Hague S, McLay K, Emmerson J, Lo C, Klaffke S, et al.** A genetic study of Wilson's disease in the United Kingdom. *Brain* 2013; 136:1476-1487.
- 22) **Seniow J, Mroziak B, Czlonkowska A, Jedryka-Goral A.** Self-rated emotional functioning of patients with neurological or asymptomatic form of Wilson's disease. *J Clin Neuropsychol* 2004; 17, 367-373.
- 23) **Zimbren PC, Schilsky ML.** Psychiatric aspects of Wilson disease: A review. *Gen Hosp Psychiatry* 2014; 36, 53-62.
- 24) **Roberts EA, Schilsky ML.** A practice guideline on Wilson disease. *Hepatology* 2003; 37,1475-1492.
- 25) **Beinhardt S, Leiss W, Stattermayer AF, Graziadei I, Zoller H, Stauber R, Maieron A, Datz C, Steindl-Munda P, Hofer H, et al.** Long-term outcomes of patients with Wilson disease in a large Austrian cohort. *Clin Gastroenterol Hepatol* 2014; 12, 683-689.
- 26) **Scheinberg IH, Gitlin D.** Deficiency of ceruloplasmin in patients with hepatolenticular degeneration (Wilson's disease). *Science* 1952; 116:484-5.
- 27) **Riordan SM, Williams R.** The Wilson's disease gene and phenotypic diversity. *J Hepatol* 2001; 34:165-71.
- 28) **Dong QY, Wu ZY.** Advance in the pathogenesis and treatment of Wilson disease. *Transl Neurodegener* 2012; 9:158-1-23.
- 29) **Kenny S, Cox DW.** Wilson disease mutation database. <http://www.medicalgenetics.med.ualberta.ca/wilson/index.php>.
- 30) **Hsi G, Cox DW.** A comparison of the mutation spectra of Menkes disease and Wilson disease. *Hum Genet* 2004; 114:165-72.

- 31) **Ferenci P.** Regional distribution of mutations of the ATP7B gene in patients with Wilson disease: impact on genetic testing. *Hum Genet* 2006; 120:151-9.
- 32) **Walshe JM.** Wilson's disease; new oral therapy. *Lancet* 1956; 270:25-6.
- 33) **Tanzi RE, Petrukhin K, Chernov I, Pellequer JL, Wasco W, Ross B, Romano DM, Pavone L, Brzustowicz LM.** The Wilson disease gene is a copper transporting ATPase with homology to the Menkes disease gene. *J Nat Genet* 1993; 5, 344-350.
- 34) **Lutsenko S, Efremov RG, Tsivkovski R, Walker JM.** Human copper-transporting ATPase ATP7B (the Wilson's disease protein): Biochemical properties and regulation. *J Bioenerg Biomembr* 2002; 34, 351-362.
- 35) **Myari A, Hadjiliadis N, Fatemi N, Sarkar B.** Copper (I) interaction with model peptides of WD6 and TM6 domains of Wilson ATPase: Regulatory and mechanistic implications. *J Inorg Biochem* 2004; 98, 1483-1494.
- 36) **Fatemi N, Sarkar B.** Molecular mechanism of copper transport in Wilson disease. *Environ Health Perspect* 2002; 110, 695-698.
- 37) **Huster D, Lutsenko S.** The distinct roles of the *N*-terminal copper-binding sites in regulation of catalytic activity of the Wilson's disease protein. *J Biol Chem* 2003; 278, 32212-32218.
- 38) **Cater MA, La Fontaine S, Mercer JFB.** Copper binding to the *N*-terminal metal-binding sites or the CPC motif is not essential for copper-induced trafficking of the human Wilson protein (ATP7B). *Biochem J* 2007; 401, 143-153.
- 39) **Tsivkovskii R, MacArthur BC, Lutsenko S.** The Lys1010-Lys1325 fragment of the Wilson's disease protein binds nucleotides and interacts with the *N*-terminal domain of this protein in a copper-dependent manner. *J Biol Chem* 2001; 276, 2334-2342.

- 40) **Dmitriev O, Tsivkoskii R, Abildgaard F, Morgan CT, Markley HL, Lutsenko S.** Solution structure of the N-domain of Wilson disease protein: Distinct nucleotide-binding environment and effects of disease mutations. *Proc Natl Acad Sci USA* 2006; 103, 5302-5307.
- 41) **Sazinsky MH, Mandal AK, Arguello JM, Rosenzweig AC.** Structure of the ATP bind domain from the *Archaeoglobus fulgidus* Cu⁺-ATPase. *J Biol Chem* 2006; 281, 11161-11166.
- 42) **Miller JV, Juul B, Maire M.** Structural organization, ion transport, and energy transduction of P-type ATPases. *Biochim Biophys Acta* 1996; 1286, 1-51.
- 43) **Moller LB, Ott P, Lund C, Horn N.** Homozygosity for a gross partial gene deletion of the C-terminal end of ATP7B in a Wilson patient with hepatic and no neurological manifestations. *Am J Med Genet* 2005; 138, 340-343.
- 44) **Braiterman L, Nyasae L, Leves F, Hubbard AL.** Critical roles for the COOH terminus of the Cu-ATPase ATP7B in protein stability, trans-Golgi network retention, copper sensing, and retrograde trafficking. *Am J Physiol Gastrointest Liver Physiol* 2011; 301: G69-G81.
- 45) **Huster D, Hoppert M, Lutsenko S, Zinke J, Lehmann C, Mossner J, Berr F, Caca K.** Defective cellular localization of mutant ATP7B in Wilson's disease patients and hepatoma cell lines. *Gastroenterology* 2003; 124, 335-345.
- 46) **Lutsenko S, Tsivkovskii R, Walker JM.** Functional properties of the human copper-transporting ATPase ATP7B (the Wilson's disease protein) and regulation by metallochaperone Atox1. *Ann N Y Acad Sci* 2003; 986, 204-211.
- 47) **Harada M, Kawaguchi T, Kumemura H, Terada K, Ninomiya H, Taniguchi E, Hanada S, Maeyama M, Koqa H, Ueno T, et al.** The Wilson disease protein ATP7B resides in the late endosomes with Rab7 and the Niemann-Pick C1 protein. *Am J Pathol* 2005; 166, 499-510.

- 48) **Gitlin JD.** Copper homeostasis: Specialized functions of the late secretory pathway. *Dev Cell* 2014; 29, 631-632.
- 49) **Polishchuk EV, Concilli M, Iacobacci S, Chesi G, Pastore N, Piccolo P, Paladino S, Baldantoni D, van IJzendoorn SC, Chan J, et al.** Wilson disease protein ATP7B utilized lysosomal exocytosis to maintain copper homeostasis. *Dev Cell* 2014; 29, 686-700.
- 50) **Cater M, la Fontaine S, Shield K, Deal Y, Mercer FBJ.** ATP7B mediates vesicular sequestration of copper; Insight into biliary copper excretion. *Gastroenterology* 2006; 130, 493-506.
- 51) **Kucinkas L, Jeroch J, Vitkauskiene A, Sakalauskas R, Petrenkiene V, Kucinkas V, Naginiene R, Schmidt H, Kupcinkas L.** High frequency of the c.3207C>A (p.H1069Q) mutation in *ATP7B* gene of Lithuanian patients with hepatic presentation of Wilson's disease. *World J Gastroenterol* 2008; 14, 5876-5879.
- 52) **Gromadzka G, Schmidt HH, Genschel J, Bochow B, Rodo M, Tarnacka B, Litwin T, Chabik G, Czonkowska A.** Frameshift and nonsense mutations in the gene for ATPase are associated with severe impairment of copper metabolism and with an early clinical manifestation of Wilson's disease. *Clin Genet* 2005; 68, 524-532.
- 53) **Cox DW, Fraser FC, Sass-Kortsak A.** A genetic study of Wilson's disease: Evidence for heterogeneity. *Am J Hum Genet* 1972; 24, 646-666.
- 54) **Lepori MB, Zappu A, Incollu S, Dessi V, Mameli E, Demelia L, Nurchi AM, Gheorghe L, Maggiore G, Sciveres M, et al.** Mutation analysis of the *ATP7B* gene in a new group of Wilson's disease patients: Contribution to diagnosis. *Mol Cell Probes* 2012; 26, 147-150.
- 55) **Roberts EA, Schilky ML.** Diagnosis and treatment of Wilson disease: An update. *Hepatology* 2008; 47, 2089-2111.

-
- 56) **Usta J, Daya HA, Halawi H, Al-Shareef I, EI-Rifai O, Malli AH, Sharara AI, Habib RH, Barada K.** Homozygosity for non-H1069Q missense mutation in *ATP7B* gene and early severe liver disease: Report of two families and a meta-analysis. *JIMD Rep* 2012; 4, 129-137.
- 57) **La Fontaine S, Mercer JFB.** Trafficking of the copper-ATPases ATP7A and ATP7B: role in copper homeostasis. *Arch Biochem Biophys* 2007; 463:149-167.
- 58) **Payne AS, Kelly EJ, Gitlin JD.** Functional expression of the Wilson disease protein reveals mislocalization and impaired copper-dependent trafficking of the common H1069Q mutation. *Proc Natl Acad Sci U S A* 1998; 95:10854-10859.
- 59) **van den Berghe PV, Stapelbroek JM, Krieger E, de Bie P, van de Graaf SF, de Groot RE, van Beurden E, Spijker E, Houwen RH, Berger R, Klomp LW.** Reduced expression of ATP7B affected by Wilson disease-causing mutations is rescued by pharmacological folding chaperones 4-phenylbutyrate and curcumin. *Hepatology* 2009; 50(6):1783-95.
- 60) **Huster D, Kühne A, Bhattacharjee A, Raines L, Jantsch V, Noe J, Schirrmeister W, Sommerer I, Sabri O, Berr F, Mössner J, Stieger B, Caca K, Lutsenko S.** Diverse functional properties of Wilson disease ATP7B variants. *Gastroenterology* 2012; 142(4):947-956.e5.
- 61) **Chandhok G, Horvath J, Aggarwal A, Bhatt M, Zibert A, Schmidt HH.** Functional analysis and drug response to zinc and D-penicillamine in stable ATP7B mutant hepatic cell lines. *World J Gastroenterol* 2016; 22(16):4109-1919.
- 62) **Dmitriev OY, Bhattacharjee A, Nokhrin S, Uhlemann E-ME, Lutsenko S.** Difference in stability of the N-domain underlies distinct intracellular properties of the E1064A and H1069Q mutants of copper-transporting protein ATPase ATP7B. *J Biol Chem* 2011; 286:16355-16362.

- 63) **Banci L, Bertini I, Cantini F, Rosenzweig A, Yatsunyk LA.** Metal binding domains 3 and 4 of the Wilson disease protein: Solution structure and interaction with the copper(I) chaperone HAH1. *Biochemistry* 2008; 47:7423-7429.
- 64) **Gitlin JD.** Wilson disease. *Gastroenterology* 2003; 125:1868-1877.
- 65) **Braakman I, Bulleid NJ.** Protein folding and modification in the mammalian endoplasmic reticulum. *Annu Rev Biochem* 2011; 80:71-99.
- 66) **Mayer MP, Bukau B.** Hsp70 chaperones: cellular functions and molecular mechanism. *Cell Mol Life Sci* 2005; 62:670-684.
- 67) **Pearl LH, Prodromo C.** Structure and mechanism of the Hsp90 molecular chaperone machinery. *Annu Rev Biochem* 2006; 75:271-294.
- 68) **Ong DS, Kelly JW.** Chemical and/or biological therapeutic strategies to ameliorate protein misfolding diseases. *Curr Opin Cell Biol* 2010; 23:231-238.
- 69) **Roth DM, Balch WE.** Modeling general proteostasis: proteome balance in health and disease. *Curr Opin Cell Biol* 2010; 23:126-134.
- 70) **D'Agostino M, Lemma V, Chesi G, Stornaiuolo M, Cannata Serio M, D'Ambrosio C, Scaloni A, Polishchuk R, Bonatti S.** The cytosolic chaperone α -Crystallin B rescues appropriate folding and compartmentalization of misfolded multispans transmembrane proteins. *J Cell Sci* 2013; 126:4160-4172.
- 71) **Kappe G, Franck E, Verschuure P, Boelens WC, Leunissen JA, de Jong WW.** The human genome encodes 10 alpha-crystallin-related small heat shock proteins: HspB1-10. *Cell Stress Chaperones* 2003; 8:53-61.
- 72) **Slingsby C, Wistow GJ, Clark AR.** Evolution of crystallins for a role in the vertebrate eye lens. *Protein Sci* 2013; 22:367-380.

- 73) **Santhoshkumar P, Murugesan R, Sharma KK.** Deletion of (54)FLRPSWF(61) residues decreases the oligomeric size and enhances the chaperone function of alphaB-crystallin. *Biochemistry* 2009; 48:5066-5073.
- 74) **Srinivas PN, Reddy PY, Reddy GB.** Significance of alpha-crystallin heteropolymer with a 3:1 alphaA/alphaB ratio: chaperone-like activity, structure and hydrophobicity. *Biochem J* 2008; 414:453-460.
- 75) **Dubin RA, Wawrousek EF, Piatigorsky J.** Expression of the murine alpha Bcrystallin gene is not restricted to the lens. *Mol Cell Biol* 1989; 9:1083-1091.
- 76) **Deretic D, Aebersold RH, Morrison HD, Papermaster DS.** Alpha A- and alpha Bcrystallin in the retina. Association with the post-Golgi compartment of frog retinal photoreceptors. *J Biol Chem* 1994; 269:16853-16861.
- 77) **Iwaki T, Kume-Iwaki A, Goldman JE.** Cellular distribution of alpha B-crystallin in non-lenticular tissues. *J Histochem Cytochem* 1990; 38:31-39.
- 78) **Bhat SP, Nagineni CN.** Alpha B subunit of lens-specific protein alpha-crystallin is present in other ocular and non-ocular tissues. *Biochem Biophys Res Commun* 1989; 158:319-325.
- 79) **Nagaraj RH, Nahomi RB, Mueller NH, Raghavan CT, Ammar DA, Petrash JM.** Therapeutic potential of α -crystallin. *Biochim Biophys Acta* 2015; 1860:252-7.
- 80) **Liu JP, Schlosser R, Ma WY, Dong Z, Feng H, Liu L, Huang XQ, Liu Y, Li DW.** Human alphaA- and alphaB-crystallins prevent UVA-induced apoptosis through regulation of PKC α , RAF/MEK/ERK and AKT signaling pathways. *Exp Eye Res* 2004; 79:393-403.
- 81) **Xu F, Yu H, Liu J, Cheng L.** alphaB-crystallin regulates oxidative stress-induced apoptosis in cardiac H9c2 cells via the PI3K/AKT pathway. *Mol Biol Rep* 2013; 40:2517-2526.

- 82) **Sreekumar PG, Kannan R, Kitamura M, Spee C, Barron E, Ryan SJ, Hinton DR.** aB crystallin is apically secreted within exosomes by polarized human retinal pigment epithelium and provides neuroprotection to adjacent cells. *PLoS One* 2010; 5:e12578.
- 83) **Treweek TM, Rekas A, Lindner RA, Walker MJ, Aquilina JA, Robinson CV, Horwitz J, Perng MD, Quinlan RA, Carver JA.** R120G alphaB-crystallin promotes the unfolding of reduced alpha-lactalbumin and is inherently unstable. *Febs J* 2005; 272:711-24.
- 84) **Garrido C, Kampinga HH, eds.** Small HSPs in physiology and pathology. *Int J Biochem cell Biol* 2012; 44(10):1587-1710.
- 85) **Bakthisaran R, Akula KK, Tangirala R, Rao Ch M.** Phosphorylation of alphaBcrystallin: role in stress, aging and pathophysiological conditions. *Biochim Biophys Acta* 2016; 1860:167-82.
- 86) **Smith JB, Sun Y, Smith DL, Green B.** Identification of the posttranslational modifications of bovine lens alpha B-crystallins by mass spectrometry. *Protein Sci* 1992; 1:601-8.
- 87) **Ahmad MF, Raman B, Ramakrishna T, Rao Ch M.** Effect of phosphorylation on alpha B-crystallin: differences in stability, subunit exchange and chaperone activity of homo and mixed oligomers of alpha B-crystallin and its phosphorylation-mimicking mutant. *J Mol Biol* 2008; 375:1040-51.
- 88) **Ciano M, Allocca S, Ciardulli MC, della Volpe L, Bonatti S, D'Agostino M.** Differential phosphorylation-based regulation of aBcrystallin chaperone activity for multipass transmembrane proteins. *Biochem and Biophys Res Com* 2016; 479(2):325-330.
- 89) **Robitaille J, MacDonald ML, Kaykas A, Sheldahl LC, Zeisler J, Dube MP, Zhang LH, Singaraja RR, Guernsey DL, Zheng B, Siebert LF, Hoskin-Mott A, Trese MT, Pimstone SN, Shastry BS, Moon RT, Hayden MR, Goldberg YP, Samuels ME.** Mutant frizzled-4 disrupts retinal angiogenesis in familial exudative vitreoretinopathy. *Nat Genet* 2002; 32:326-30.

- 90) **Ecroyd H, Meehan S, Horwitz J, Aquilina JA, Benesch JL, Robinson CV, Macphee CE, Carver JA.** Mimicking phosphorylation of alphaB-crystallin affects its chaperone activity. *Biochem J* 2007; 401:129-41.
- 91) **Ghosh JG, Houck SA, Clark JI.** Interactive sequences in the molecular chaperone, human aB crystalline modulate the fibrillation of amyloidogenic proteins. *Int J Biochem cell Biol* 2008; 40:954-967.
- 92) **Bhattacharyya J, Padmanabha U, Wang J, Sharma KK.** Mini-aB-crystallin: a functional element of aB crystalline with chaperone-like activity. *Biochemistry* 2006; 7:3069-3076.
- 93) **Sreekumar PG, Chothe P, Sharma KK, Baid R, Kompella U, Spee C, Kannan N, Manh C, Ryan SJ, Ganapathy V, Kannan R, Hinton DR.** Antiapoptotic Properties of a-Crystallin-Derived Peptide Chaperones and Characterization of Their Uptake Transporters in Human RPE Cells. *Invest Ophthalmol Vis Sci* 2013; 54:2787-2798.
- 94) **Nahomi RB, Wang B, Raghavan CT, Voss O, Doseff AI, Santhoshkumar P, Nagaraj RH.** Chaperone Peptides of a-Crystallin Inhibit Epithelial Cell Apoptosis, Protein Insolubilization, and Opacification in Experimental Cataracts. *J Biol Chem* 2013; 288:13022-13035.
- 95) **Chandhok G, Schmitt N, Sauer V, Aggarwal A, Bhatt M, Schmidt HH.** The effect of zinc and D-penicillamine in a stable human hepatoma ATP7B knockout cell line. *PLoS One* 2014; 9(6):e98809.
- 96) **Okita K, Matsumura Y, Sato Y, Okada A, Morizane A, Okamoto S, Hong H, Nakagawa M, Tanabe K, Tezuka K, Shibata T, Kunisada T, Takahashi M, Takahashi J, Saji H, Yamanaka S.** A more efficient method to generate integration-free human iPS cells. *Nat Methods* 2011; 8(5):409-12.
- 97) **Si-Tayeb K, Noto FK, Nagaoka M, Li J, Battle MA, Duris C, North PE, Dalton S, Duncan SA.** Highly efficient generation of human hepatocyte-like cells from induced pluripotent stem cells. *Hepatology* 2010; 51(1):297-305.

- 98) **Asomugha CO, Gupta R, Srivastava OP.** Structural and functional roles of deamidation of N146 and/or truncation of NH₂- or COOH-termini in human α B-crystallin. *Mol Vis* 2011; 17:2407-2420.
- 99) **Raju M, Santhoshkumar P, Sharma KK.** Alpha-crystallin-derived peptides as therapeutic chaperones. *Biochim Biophys Acta* 2015; 1860(1 Pt B):246-51.
- 100) **Gordon GW, Berry G, Liang XH, Levine B, Herman B.** Quantitative fluorescence resonance energy transfer measurements using fluorescence microscopy. *Biophys J* 1998; 74(5):2702-13.
- 101) **Leavesley SJ, Rich TC.** Overcoming limitations of FRET measurements. *Cytometry A* 2016; 89, 325-7.
- 102) **Kannan R, Sreekumar PG, Hinton DR.** Novel roles for α -crystallins in retinal function and disease. *Prog Retin Eye Res.* 2012; 31:576-604.
- 103) **Zhang S, Chen S, Li W, Guo X, Zhao P, Xu J, Chen Y, Pan Q, Liu X, Zychlinski D, Lu H, Tortorella MD, Schambach A, Wang Y, Pei D, Esteban MA.** Rescue of ATP7B function in hepatocyte-like cells from Wilson's disease induced pluripotent stem cells using gene therapy or the chaperone drug curcumin. *Hum Mol Genet* 2011; 20(16):3176-87.
- 104) **Yi F, Qu J, Li M, Suzuki K, Kim NY, Liu GH, Belmonte JC.** Establishment of hepatic and neural differentiation platforms of Wilson's disease specific induced pluripotent stem cells. *Protein Cell* 2012; 3(11):855-63.
- 105) **Jucker M.** The benefits and limitations of animal models for translational research in neurodegenerative diseases. *Nat Med* 2010; 16(11):1210-4.
- 106) **Huch M, Koo BK.** Modeling mouse and human development using organoid cultures. *Development* 2015; 142(18):3113-25.

- 107) **Stapelbroek JM, Bollen CW, van Amstel JK, van Erpecum KJ, van Hattum J, van den Berg LH, Klomp LW, Houwen RH.** The H1069Q mutation in ATP7B is associated with late and neurologic presentation in Wilson disease: results of a meta-analysis. *J Hepatol* 2004; 41(5):758-63.
- 108) **Chesi G, Hegde RN, Iacobacci S, Concilli M, Parashuraman S, Festa BP, Polishchuk EV, Di Tullio G, Carissimo A, Montefusco S, Canetti D, Monti M, Amoresano A, Pucci P, van de Sluis B, Lutsenko S, Luini A, Polishchuk RS.** Identification of p38 MAPK and JNK as new targets for correction of Wilson disease-causing ATP7B mutants. *Hepatology* 2016; 63(6):1842-59.

8. LIST OF PUBLICATIONS

- Ciano M*, **Allocca S***, Ciardulli MC, della Volpe L, Bonatti S, D'Agostino M. Differential phosphorylation-based regulation of aBcrystallin chaperone activity for multipass transmembrane proteins. *Biochemical and Biophysical Research Communications*. 479(2): 325-330. 2016 October 14. PMID: PMC505354.

* These authors contributed equally to this work

- **MANUSCRIPT SUBMITTED**
Parisi S, Polishchuk EV, **Allocca S**, Ciano M, Musto A, Gallo M, Perone L, Ranucci G, Iorio R, Polishchuk RS, Bonatti S. Characterization of the most frequent ATP7B mutation causing Wilson disease in hepatocytes derived from patient induced pluripotent stem cells.